Biofidelity Evaluation of Thoracolumbar Spine Model in THUMS

Master's thesis in Biomedical Engineering

HENOK AFEWERKI

Department of Applied Mechanics
Division of Vehicle Safety
CHALMERS UNIVERSITY OF TECHNOLOGY
Gothenburg, Sweden 2016

Master's thesis in biomedical engineering

Biofidelity Evaluation of the Thoracolumbar Spine Model in THUMS

HENOK AFEWERKI

Department of Applied Mechanics
Division of Vehicle Safety
Chalmers University of Technology
Gothenburg, Sweden 2016

Biofidelity Evaluation of the Thoracolumbar Spine Model in THUMS
HENOK AFEWERKI

Supervisor: Johan Ireaus and Mats Y. Svensson
Examiner: Karin Brolin

Master's Thesis 2016:54
ISSN 1652-8557
Department of Applied Mechanics
Division of Vehicle Safety
Chalmers University of Technology
SE-412 96 Gothenburg
Sweden
Telephone +46(0)31-772 1000

Cover: Thoracolumbar spine model in THUMS ALR, Section 5.2

Typeset in LaTeX
Department of Applied Mechanics
Gothenburg, Sweden 2016

Biofidelity Evaluation of the Thoracolumbar Spine Model in THUMS
Master's thesis in Biomedical Engineering
HENOK AFEWERKI
Department of Applied Mechanics
Division of Vehicle Safety
Chalmers University of Technology

ABSTRACT

Thoracolumbar spine injuries in motor vehicle crashes are occurring and the mechanisms are poorly understood. It has been hypothesized to be connected to vehicle's restraint systems but further studies are required to understand and subsequently address the problem in future restraint systems. Finite Element (FE)-Human body models are invaluable tools for crash analysis, however, quality of the response depends on the biofidelity of the model. The objective of this thesis is to evaluate biofidelity of the thoracolumbar spine model in Total Human Model for Safety (THUMS), Toyota Motor Corporation and Toyota Central R&D Labs .

In this thesis work three dynamic and one static thoracolumbar experiments were simulated. THUMS' ligaments were verified against cadaveric data. Two modified disc material models were inserted in to THUMS and the results compared against experimental data. The Global Human Body Model Concertium model (GHBMC), GHMBC, LLC was also evaluated against cadaveric data from two experiments. All simulations were run in LS-DYNA and pre and postprocessing tasks were performed in LS-PrePost and Matlab.

The response of the lumbar FSUs in THUMS' under the dynamic compression test was similar to the experimental data but was three to four times less stiff. On the other hand, the T12-L5 segment showed fair correlation of reaction force whereas reaction moment was significantly lower. Kinematics of the cadaveric spine under flexion and extension tests was not captured. Reaction moment, shear force and vertical displacement were found to deviate from the response of the cadaveric specimens during the dynamic flexion and shear test. Only horizontal displacement showed good correlation in this test. THUMS performance was good in the static flexion and shear test but poor in flexion only test. Furthermore, the Capsular Ligaments (CL) and the Ligamentum Flavum (LF) in THUMS were found to be about three times shorter and stiffer, respectively. In all the simulations the intervertebral contacts were responsible for the sudden and large increase and vibrations occurring at about the experimental failure point. The modified disc material models improved response of only the lumbar FSUs under the compression test.

In conclusion, biofidelity of the thoracolumbar spine model in THUMS is found to be poor and remodelling is necessary. The compliant nature of the intervertebral discs, the shorter length of the CL and higher stiffness of the LF and the smaller initial inveterver-tebral gap were identified as the main weaknesses of the model.

Keywords: Thoracolumbar, Biofideltiy, Kinematics, Flexion, Extension, Shear, Stiffness

Preface

This masters thesis is the final part of the Master of Science in Biomedical Engineering at Chalmers University of Technology. It was carried out at the SAFER Vehicle and Traffic Safety Center at Chalmers, Göteborg, Sweden, under the supervision of Johan Ireaus and Mats Y. Svensson. The examiner was Karin Brolin, at the Division of Vehicle Safety, Department of Applied Mechanics at Chalmers University of Technology.

Acknowledgement

First and foremost I would like to thank God for everything I have and everything that was made available to me. Following this, my utmost gratitude goes to my examiner Karin Brolin and my supervisors Johan Ireaus and Mats Y. Svensson without which nothing would be possible. I am deeply indebted to the knowledge you communicated and patience you showed throughout the time duration. Thanks to Lotta Jakobsson for the opportunity and resources. Also my appreciations to Jonas Östh for his invaluable help and guidance. Thanks to all the wonderful people at SAFER and Volvo Cars that made my stay enjoyable.

Contents

List of Figures

List of Tables

Definitions and Abbrevations

THUMS	Total HUman Model for Safety (Toyota Motor Corporation and Toyota Central R&D Labs)[1][2].
FE	Finite Element.
GHBMC	Global Human Body Model Consertium [3].
LS-DYNA	A general purpose finite element program capable of simulating real worldproblems (Livermore Software Technology Corporation, Livermore, CA).
LS-PrePost	A freely distributed pre and post processor (Livermore Software Technology Corporation, Livermore, CA).
FSU	Functional Spinal Unit.
CL	Capsular ligament.
LF	Ligamentum Flavum.
MVCs	Motor Vehicle Crashes.
NASS-CDS	National Automotive Sampling System-Crashworthiness Data System [4].
CIREN	Crash Injury Research & Engineering Network [4].
PMHS	Post Mortem Human Subject.
ATD	Anthropomorphic Test Device, crash test dummy.
C1,C2,...C7	cervical vertebral bones number 1 to 7.
T1, T2,...T12	The thoracic vertebral bones number 1 to 12.
L1, L2,...L5	The lumbar vertebral bones number 1 to 5.
lordosis	Inward curvature of the lumbar and cervical spines.
kyphosis	Outward curvature of the thoracic spine.
ALL	Anterior Longitudinal Ligament.
PLL	Posterior Longitudinal Ligaments.
SSL	SupraSpinous Ligament.
ISL	IntraSpinous Ligament.
ITL	IntraTransverse Ligament.
AIS	Abbreviated Injury Scale, an anatomically based, consensus derived, global severity scoring system classifying body region injury on a 6-point ordinal scale (1=minor and 6=maximal) [5].
SAFER	Vehicle and Traffic Safety Center at Chalmers.
SM2S	Spine Model for Safety and Surgery [6].

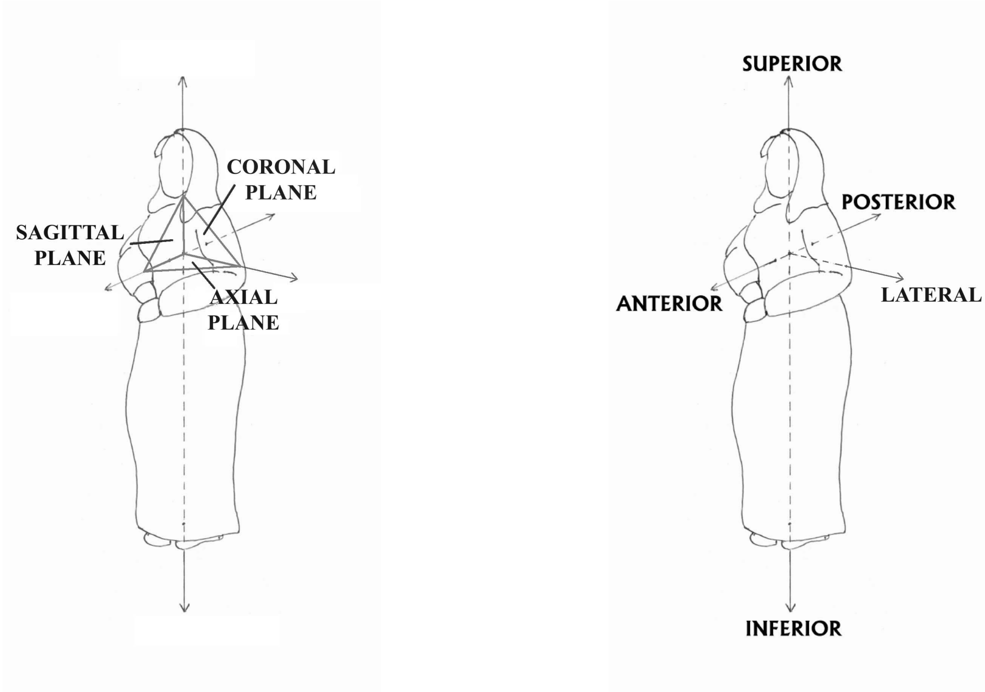

(a) **(b)**

Figure 0.1: Anatomical planes and axes [Courtesy of Karin Brolin] [7]

1

Introduction

The introduction and evolution of motor driven machines have greatly simplified our life by promoting manufacturing speed, human comfort and accelerating industrialization. Humans have benefited from this technological advancement and enjoyed a transformed life style. On the other hand distressing number of injuries and fatalities are imparted by the same machines every year. Road traffic accidents alone claim 1.3 million lives and impart severe injuries on 50,000,000 citizens every year [8]. It is forecasted to rise by 66% by 2020 [9].

Injury prevention and crash avoidance are in a continuous progress combating unintentional injuries sustained every day. Active safety aims at avoiding crashes and is instrumental in slow to average speed motor vehicle crashes. However, given the brevity of high speed crashes and the difficulty to overcome the induced forces and momentus many crashes fall far from the realm of active safety. Passive safety goes an extra mile in protecting occupants when crashes become unavoidable [10].

One of the earliest passive safety measures to counteract vehicle traffic injuries was the introduction of the three point seat belts in 1959 by Bohlin, Volvo car corporation, Sweden [11] which is estimated to have saved more than one million lives in the past four decades. Later in history the evolution of restraint systems, seats, airbag, side airbag, pedestrian airbag and so forth further dropped injury and fatality rates in Motor Vehicle Crashes (MVCs).

While this holds for majority of the body parts, a rising number of thoracolumbar injuries has recently been documented. Jakobsson et al (2006) [12] conducted a retrospective study on 21,034 Volvo car accidents in Sweden between the year 1995 and 2005. The report disclosed that out of 189 thoracolumbar injury cases, a significant reduction in thoracolumbar injury risk for MAIS 2+ but only an insignificant reduction for AIS 2+ in newer car models as compared to older models. A similar study [13] queried the NASS-CDS and CIREN databases for thoracolumbar injuries between the year 1993 and 2010. The result showed a slightly rising trend in thoracolumbar injuries during frontal crashes as a function of vehicle model year. This trend is continuing in 2015 [14].

Thoracolumbar injuries sustained during MVCs and traffic accidents share 0.3% to 2% of all other body injuries [15]. Nevertheless they are still responsible for more than 50% of the total thoracolumbar injuries from different activities [16][17][18] and are typically severe and disabling [19]. Despite all this only little attention is given to the thoracolumbar spine injury. Only 8% of all spinal column experiments from 1990 to 2009 are thoracolumbar spine experiments with majority being lumbar spine experiments [20], as a consequence mechanisms of the thoracolumbar injury have been poorly understood [21].

Understanding interaction of human body with the vehicle environment during crashes is the first and necessary step in the design of restraint systems in passive safety. Moreover, the fact that different body parts are loaded differently under a single impact and the inherent difference in tolerance levels between different body part require a separate body part by part study. Vehicle safety researches have been carried out with human volunteers, Post Mortem Human Subject (PMHS) and Anthropomorphic Test Device, crash test dummy (ATD) and consequently running cost has been quite detrimental. On the other hand, volunteers can not be subjected to risky scenarious and experimenting on PMHS is ethically criticized and desired attributes such as age, height and weight are hardly available when needed.

ATDs are designed for repeatablity and thus are only crude representation of the human body. Mathematical Finite Element (FE)-models are potential substitutes in this case. With FE models crash analysis becomes easier. Today many different human body FE models for safety are available. While, in general, they are capable of simulating kinetic and kinematic responses during crashes, quality of the attained response is dependent upon degree of biofidelity of the model. Therefore biofidelity evaluation of a human body model is a necessary step to assess trustworthiness of a model.

One popular human body model is the Total HUman Model for Safety (Toyota Motor Corporation and Toyota Central R&D Labs)[1][2] (THUMS) [1][2]. THUMS has been used for crash analysis by vehicle and research industries since its first release in 1997. It is validated in fullbody and body part level against human cadaveric data. Valdiation of the cervical spine model in THUMS has been conducted in two studies [22][23]. However, to my best knowledge, the thoracolumbar spine has been disregarded and no validation or evaluation work has been reported to date.

1.1 Aim

The aim of this thesis work is to evaluate biofidelity of the thoracolumbar spine model in THUMS. The models response at experimental failure point under major loading modes, and kinematics are the focus of this evaluation work. This thesis is expected to help determine if the model is biofidlic enough to be used for injury prediction in frontal crashes. Hence the focus is on compression, flexion and shear loading.

1.2 Limitations

This thesis work was limited to the evaluation of the thoracolumbar spine of THUMS versions 1.4, 3.0 and a modified version of THUMS 1.4 [24][25] as they are identical models. Any other FE model including other versions of THUMS are not part of this evalutation.

Because of the limited number of cadaveric expriments the evaluation work is further limited to only isolated specimens. Well defined full cadaveric experiments with spinal measurements were not found and not simulated. It should be noted that isolated specimens do not include the effect of other body parts on the stiffness and biofidelity of the thoracolumbar spine. For example the abdominal pressure and the muscles force, which are known to influence the response of the spine, are abscent.

For the intended purpose, the model is biofidelic if good correlation is obtained at failure point regardless of the response outside the failure region. However, in THUMS failure is not implemented in the material models or through element elimination. Therefore, a second paratemeter, such as flexion angle, time or displacement were used to predict failure in the model.

2

Anatomy of the Thoracolumbar Spine

Human spine, also called the vertebral column is a complex part of the skeletal system that supports the upper body and protects the spinal cord from injury. It is composed of 33 vertebral bones in a chain like fashion, extending from just below the skull to the coccyx in the pelvis region. The spine facilitates upper body locomotion and is therefore flexible and not strong enough to withstand high rate mechanical insults from modern day transport systems [19]. The sigmoid shape of the spine in the saggital plane, has mechanically advantage [10].

Human spine is commonly classified as cervical, thoracic, lumbar, sacral and coxycal units in order from superior to to inferior end, see Figure 2.1. They are repeated structures of vertebral bones and intervertebral discs connected end to end. At the very superior edge of the spine is the first of the seven cervical vertebral bones (C1,C2,...C7). The thoracic spinal unit consists of the next 12 vertebral bones (T1, T2,...T12) and corresponding soft tissues. The largest five vertebral bones and their soft tissues together form the lumbar spine (L1, L2,...L5) which comes directly after the thoracic spine. The last spade shaped structure at lower end of the spine consists of 5 fused vertebral bones of the sacrum and 4 fused bones of the coccyx.

Cervical and lumbar spines are longer anteriorly than posteriorly exhibiting backward curve known as lordosis [26]. The opposite of this is the kyphosis, forward curve at the thoracic and sacral spines, see Figure 2.1. The smallest functional unit of the spinal column is called a Functional Spinal Unit (FSU). The FSU consists of to two adjacent vertebral bones, an intermediate intervertebral disc and the corresponding soft tissues. Thoracolumbar spine is a collective name given to the thoracic and lumbar spinal units. Likewise, soft tissues refers to the intervertebral discs, fibers, ligaments, muscles and other non bony (soft) tissues.

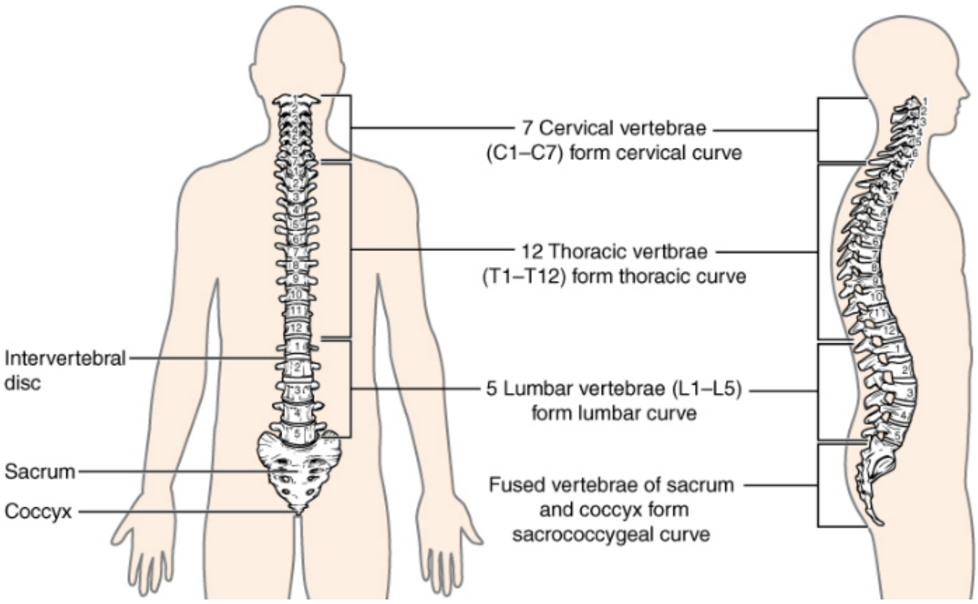

Figure 2.1: Anatomy of the human spine, [OpenStax, Rice University] [27]

2.1 Vertebral bones

Each vertebral bone is made up of an outer casing of compact bone (cortical bone) and an inner spongy (cancellous) bone. A single vertebral bone consists of a large central vertebral body and several posterior projections. The vertebral bone is roughly cylindrical with a kidney shaped cranial and caudal surfaces and concave shaped outer rims [26]. Thoracic vertebrae are smaller in size than the lumbar vertebrae but has longer spinous processes, see Figure 2.2. Lumbar vertebras are 40-50 mm in saggital width and 30-35 mm in longitudinal height [26]. At the cranial and caudal aspects of each vertebral body are thin cartilagenous bones called endplates, mean height 0.6 mm. Endplats serve as attachment points between the intervertebral discs and the vertebral bodies [10].

Posterior projections from the vertebral body are called posterior elements. These are the pedicles, lamina, spinous process, articular process, transverse process and the rib attachment bone of the thoracic spine, see Figure 2.3. Pedicles are attached to the vertebral body. The laminas are quadrilateral shaped posterior extensions extending backward from the pedicles. Attached to the common point of the two backward converging laminas and extending posteriorly is the spinous process. Transverse process is a lateral projection originating at the pedicles.

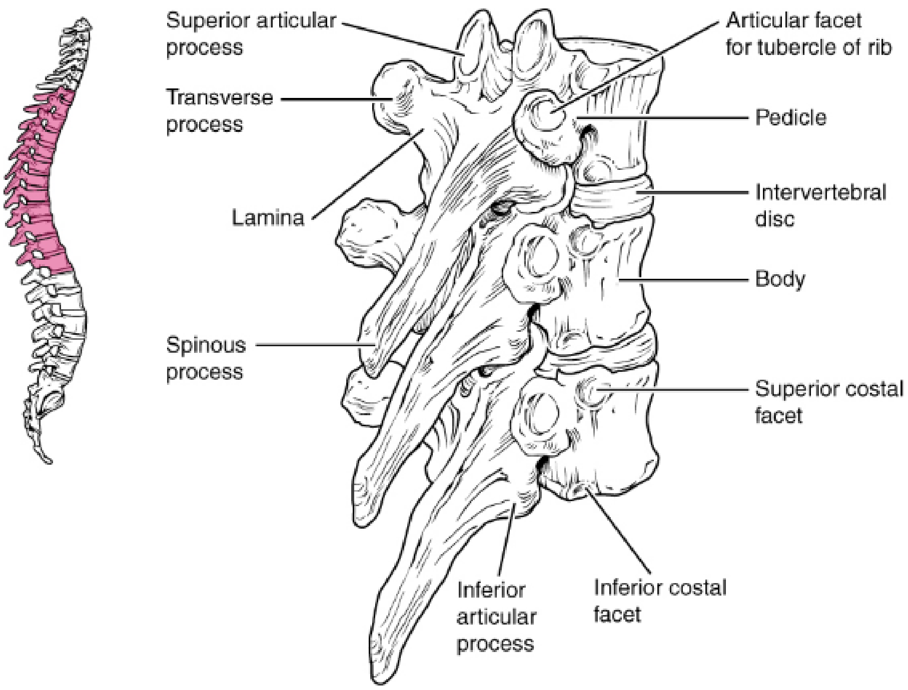

(a) Thoracic vertebrae

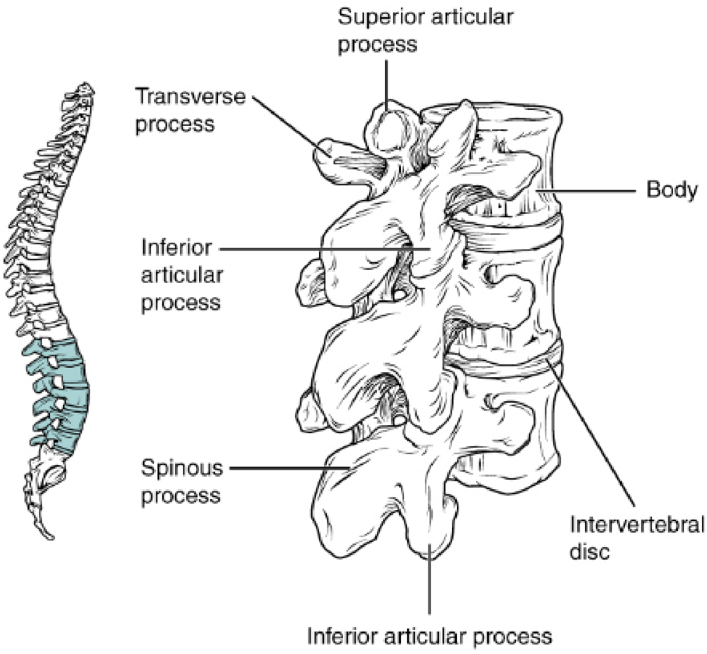

(b) Lumbar vertebrae

Figure 2.2: Thoracic and lumbar vertebrae [OpenStax, Rice University] [27]

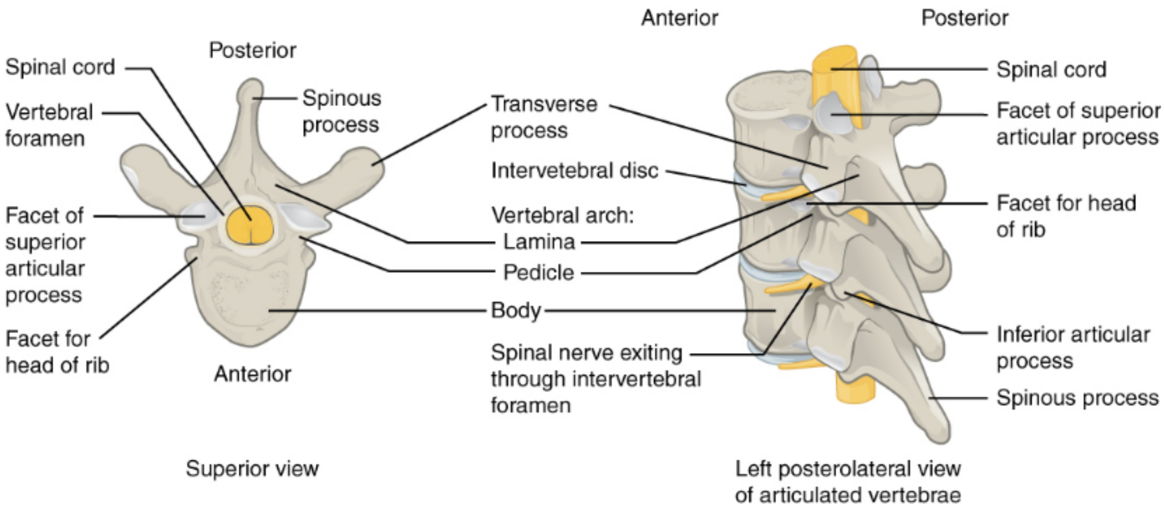

Figure 2.3: Parts of a typical vertebra, [OpenStax, Rice University] [27]

The arch formed by the vertebral body, the medial aspect of the pedicles, the laminas and the articular processes is called the vertebral foramen, see Figure 2.3. It forms the spinal canal where the spinal cord is protected from injury. Spinal cord roots leave the spinal canal via the intervertebral foramen which is a lateral arch between pedicles of two adjacent vertebrae.

2.2 Intervertebral discs

Intervertebral discs are soft tissues structures connecting adjacent vertebral bones. A single intervertebral disc is made up of a soft and highly elastic nucleus pulposus located at the center (more posteriorly), stiffer peripheral annulus fibrosus and the disc fibers, see Figure 2.4. Nucleus pulposus is incompressible semi fluid mass [26]. Annulus fibrosus is made up of concentric layers with fibers. Disc fibers connect an intervertebral disc to a vertebral body. They are more abundant at the outer rim of the annulus than at the annulus and nuclues junction. Attachment between an intervertebral disc and a vertebral body is further strengthened by the endplates and ligaments [10].

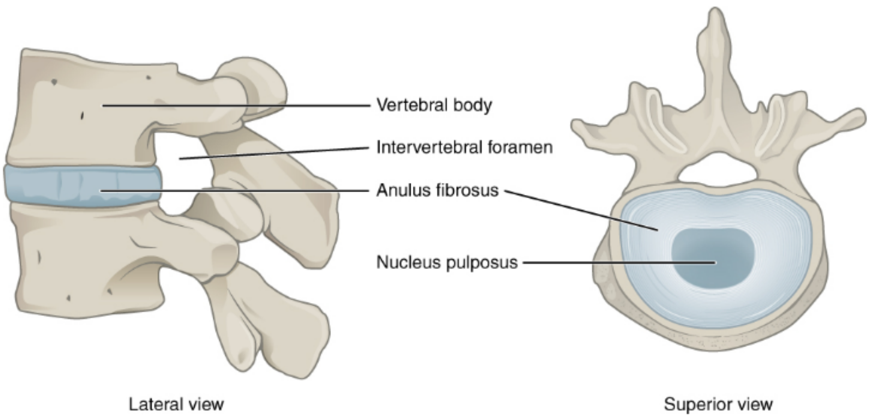

Figure 2.4: Intervertebral disc [27]

Lumbar discs have greater anterior height hence the lordotic curve whereas thoracic discs are longer posteriorly than anteriorly and are, in general, shorter than the cervical and lumbar discs. Intervertebral discs are major load propagating structures between two adjacent vertebral bones. Intervertebral discs of the lumbar spine resists axial compression and tension, anterio-posterior shear and axial rotation. Similarly the thoracic discs resist forces in all direction but primary axial compression [10]. Average length of a lumbar discs is 10 mm [26].

2.3 Ligaments

Ligaments are uniaxial structures composed of elastin and collagen materials and reacting in tension. Stretched ligament have stored elastic energy which is released during unloading. There are seven spine ligament types, five of which are extend over two adjacent vertebral bones only while the remaining cover several vertebrae.

Anterior Longitudinal Ligament (ALL) and Posterior Longitudinal Ligaments (PLL) are the longest ligaments in the spinal column. ALL is composed of collagen fibers and have three layers. The inner layer attaches the edges of two adjacent discs. The middle layer connects discs and their vertebral bodies over three layers. The superficial layer spans four to five vertebral bodies. ALL controls extension response of the spine. On the posterior end of the vertebral body is a PLL. The deepest fibers of the PLL connect only two adjacent vertebral bodies whereas the stronger superficially located fibers extend over several layers. PLL closely adheres to the discs while only marginally to the vertebral bodies. It is thicker over the thoracic region and controls flexion response of the spine.

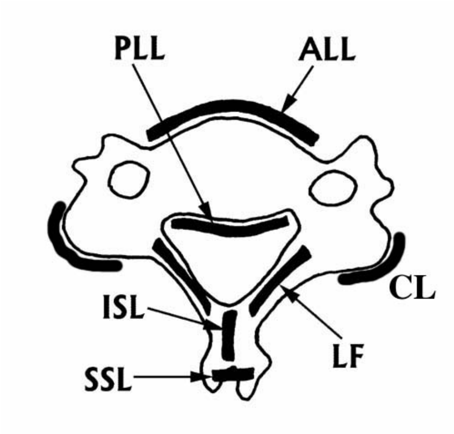

Figure 2.5: location of the vertebral ligaments [Courtesy of Karin Brolin] [7]

With 80% elastin content, the Ligamentum Flavum (LF) is one of the most elastic ligaments. It is always under pretension to maintain functional spinal unit and therefore is effective in returning lamina to neural position following flexion. LF is attached to the anterior edge of the inferior lamina and the posterior edge of superior lamina and is discontinuous at the mid vertebral body level [28].

Two articular facets are joined by the Capsular ligament (CL). CL encapsulates the facet joints with primary purpose of limiting joint distraction and sliding. CL resists hyperflexion.

SupraSpinous Ligament (SSL) connects spinous processes from two adjacent vertebras at the distal tip. SSL resists flexion response of the spine. ISL connects inner length of two adjacent spinous processes. ISL is located between the LF and SSL and resists mainly flexion response. IntraTransverse Ligament (ITL) connects two transverse processes in adjacent vertebras. ITL resists rotation and lateral bending.

2.4 Facet joints

Facet Joints are formed between the opposing surfaces of the inferior and superior articular processes of two adjacent vertebrae. Orientation of the facet joint is dorso-medially for the caudal process and ventro-laterally for the cranial articular processes [26]. This orientation is particularly important for how the facets share part of the spinal load. Average crossectional area of the facet joints at the lumbar spine is 1.6cm^2 [26].

Facet joints are capable of resisting compressive forces but not tensile forces [10]. During compression 0-33% of the force is absorbed by the facet joints [29][19][30]. On the other hand, the facet joints provide little support during lateral bending while again actively resisting axial rotations [18]. Furthermore hyperextended spine is reported to transfer more loads to the facet joints than erect spine [30].

3
Biomechanics of the Thoracolumbar Spine

Spine loads are linear forces and/or rotational moments. Linear forces can be applied in any direction but are, in general, classified in to compression, tension and shear, see Figure 3.1. Axial (compression and tension) forces are applied parallel to the longitudinal axis and perpendicular to the transverse plane. Anterior and posterior shear is perpendicular to the coronal plane whereas lateral shear is perpendicular to the sagittal plane. Likewise bending moment can be flexion or extension in the sagittal plane, lateral flexion in the coronal plane and axial torsion in the transverse plane [10].

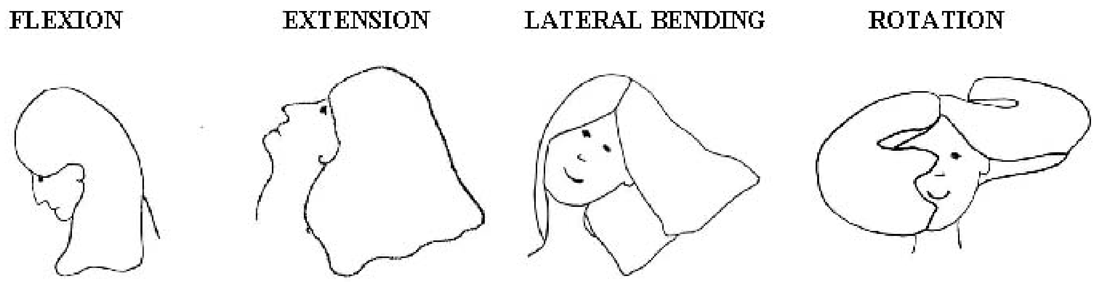

(a) Direction of moments

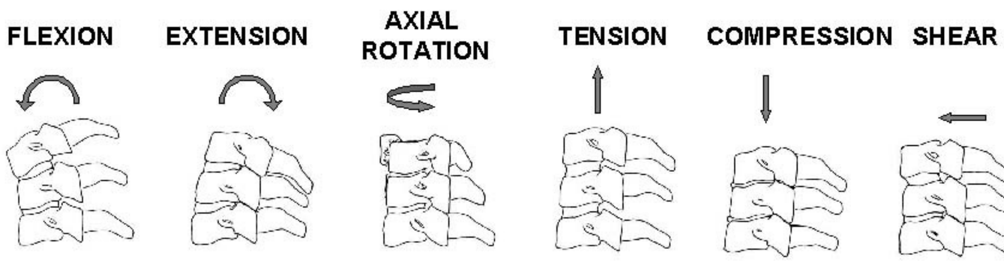

(b) Direction of forces

Figure 3.1: Spinal Forces and Moments. [Courtesy of Karin Brolin] [7]

Biological tissues under mechanical load deform until the physiological limit is reached. Injury is said to be sustained once physiological limit is exceeded. Range of motion of a lumbar FSU is $12 - 16\,\text{deg}$ in flexion/extension, $6\,\text{deg}$ lateral bending, $2\,\text{deg}$ in axial rotation and $0.1 - 1.9$ mm in tension, compression and shear [26].

In reality pure mechanical loads are rare. Loads are usually coexisting with some more dominant than others depending on the activity. Typical injury causing activities are motor vehicle crash, pilot seat ejection, under body blast, fall from height, parachuting, skiing, horse kicks, helicopter crash, and spaceship launching.

Injuries from MVCs are due to the gross sudden acceleration of the body during impact. Majority of thoracolumbar injuries are compression related and occur in frontal crashes. In a plain frontal crash, a vertical load is reported to propagate from the car chassis to the pelvis via the seatpan, leading to burst and/or wedge fractures [31][13]. The L1 and T12 vertebrae are the most injured in the thoracolumbar spine [13].

Munjin et al 2011 [32] studied thoracolumbar injuries sustained by rear bus passengers. They reported that 3 out of 5 patients sustained compression fractures. Mechanism of injury is hypothesized to be due to lifting up and down of the passangers as bus traverses speed bumps. 65% of the subjects in this study sustained thoracolumbar junction injury [32]. Similarly, thoracolumbar injuries in roll over crashes occur from occupants interacting with the vehicle's roof. It is common for lap and shoulder belted occupants. Although the C5 to C7 vertebrae is most injured, compression related injuries are also reported for the T1-T4 vertebrae [33]. Only 1% of the injuries are ligament injuries. Occupants of roll over crashes were more likely to sustain transverse process, lamina and facet fractures [33].

On the other hand, high speed boat crewman in naval military operations are reported to sustain compression related thoracolumbar injuries [34]. A retrospective study by Nikoll et al 1949 [35] on mine workers with thoracolumbar injury reported hyperflexion coupled with posterior-anterior shear as the mechanism of injury. Common injury site was found to be between T12 and L2 [35]. Similarly, in parachuting main cause of injury is impact with the ground [36].

From the above typical injurious activities it can be concluded that the dominant loading mode in MVCs leading to thoracolumbar injuries is compression and that thoracolumbar junction is the main injury site.

3.1 Characteristics of the thoracolumbar spine injuries in MVCs

Although mechanisms of thoracolumbar injuries are not perfected several studies exist that gives good insight in to the problem. More than 50% of the total thoracolumbar injuries are from MVCs [16]. More than half of this occur at the thoracolumbar junction. This is hypothesized to be due to the change in curvature from lordosis to kyphosis [32] and due to the dramatic increase of the facet sagittal orientation between T12 and L1 [37].

Frontal impacts were responsible for more thoracolumbar injuries than all other impact types together for crashes between the year 1993 and 2010 with the exception of 2002 [13]. Compression was identified as the main loading mode. similarly, lumbar spine of a three point seat belt restrained THOR in frontal impact was found loaded mainly under compression accompanied by anterior shear and flexion moment [38].

On the other hand the effect of the three point seat belts on the thoracolumbar spine injury is unsettled. Retrospective study from the regional spinal cord injury center predicted that occupants restrained by three point lab belt are more likely to sustain spinal burst fractures but are protected against abdominal injuries and flexion distraction [39]. On a similar study seat belts and airbags were protective against cervical and thoracic spines but not lumbosacral spine [40]. Meanwhile, Inamasu et al 2007 [17] reported efficacy of three point seat belts in reducing flexion distraction and neurologic injuries in the thoracolumbar spine. Furthermore, Rae et al 2014 [41] underlined the use of three point seatbelt in reducing injury severity, fatality and flexion distraction but also the associaciation with the increasing trend in thoracolumbar injuries.

A comprehensive retrospective study on the effect of restraint systems on thoracolumbar injuries during frontal crashes of restrained occupants was conducted in 2006 by Richards et al [15]. Statistical data from National Automotive Sampling System-Crashworthiness Data System [4] (NASS-CDS) database (1995-2004) for three point restrained occupants with and without deployed airbags sustaining AIS 2+ and AIS 3+ injuries and data from sled and vehicle crash experiments using ATDs were combined. In the study, the NASS-CDS database revealed that 80% of these impacts occurred at delta-v less than 37km/h. AIS 2+ injuries accounted for less than 0.6% of the total number of three point restrained occupants for severity less than 40km/hr but are quite pronounced (10.3%) for severity speeds above 60km/hr. AIS 3+ injuries were less than 1% for all severity. In both cases airbag were protective for moderate severity but quite the contrary for high severity crashes. Furthermore 35% for delta-v less than 40km/hr and 50% for severity greater than 60% of occupants also sustained abdominal injury. Combining these findings the authors concluded that the rising number of thoracolumbar injuries can only be blamed on the improper use, rather than inefficacy, of the restraint systems.

On the other hand critical factors influencing injury severity and type are discussed. The relevant ones are the crash severity, age, bone degeneration and loading rate. 73% of the total cases of thoracolumbar injury sustained in pure frontal crashes (with no following crashes), with optimal positioned occupants occur at severity speeds below 56km/hr [13].

Literature review on thoracolumbar spine segments under compressive load was conducted [42]. The result disclosed that specimens from cadavers exceeding 60 years had 50% less tolerance than younger cadaveric specimens. On another study specimens from a 70 years old cadavers collapsed under compressive load while a specimens of a 40 years old sustained burst fractures [29]. Shirado later confirmed the reduced likelihood of burst fractures in degenerated and osteorporotic spine [37].

Loading rate dependence of the cortical bone was identified as early as in 1976, similarly, rate dependency of ligaments is identified in Neumman et al 1992 [43]. Osvalder et al 1993 [44] and Neuman et al 1993 [45] reported that specimens (lumbar FSUs) could tolerate higher loads at higher loading rates but injury occurred at lower deformations [44]. Similar findings are reported in [46][47][48]. Furthermore burst fractures are formed under high rate compressive loading while the same loading at lower rate leads to other type of injury [10][49].

A pre-flexed spine has a relatively lower fracture tolerance than an erect spine [49]. On the other hand, a pre-extended spine increased fracture tolerance [37][50]. Similarly lumbar FSUs are found to be at least twice as stiff in extension than in flexion [51]. The T12-L5 segment from 11 human cadavers were found to be on average 29 times stiffer in extension than flexion without the muscles but 57% more flexible when muscles are simulated in an in vitro study conducted in Wayne State University [50][47]. The general hypothesis for increased tolerance in hyperextension is the eccentricity of the center of gravity of the head and torso is responsible for transferring greater loads to the facets [30].

3.2 Mechanism of the thoracolumbar injuries

Spine injuries have been categorized based on different criteria's and purposes. Denis et al's 1983 [52] classification targeted to standardize clinical treatment and was mainly focused on the stability of the injured spine. Magerl et al's 1994 [53] comprehensive classification was based on pathmorphological data and loading modes. Nikoll et al 1949 [35] laid down spine injuries as observed in mine workers. Stemper et al 2015 [10] categorized thoracolumbar injuries common in MVC. Spine injuries in frontal and vertical decelerations are further studied by King et al 2002 [19]. Finally common thoracolumbar injuries in Volvo car crashes are reported by Jakobsson et al 2006 [12]. Summary of thoracolumbar spine injury classifications and mechanisms from the last three studies [10][12][19] are presented below.

3.2.1 Burst fractures

Three column classification burst fracture involves injury to the anterior and middle column of the spine [52]. This type of injury may also disturb posterior elements of the vertebral without affecting the ligaments therefore the spine remains stable as a whole. Kifune et al 1995 [18], however, observed that these fractures were unstable under any circumstance.

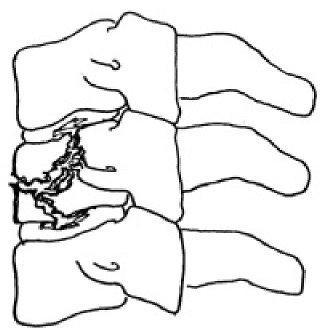

Figure 3.2: Burst fractures [Courtesy of Karin Brolin] [7]

Burst fractures are due to compressive forces applied along the axis of vertebral body. Early during axial compression of the spinal column, the discs start to lose volume. With the continued application of axial force the end plates bulge and eventually fail. This is because the end plates are more porous than the annulus fibrosis. End plates are reported to fail first for a compressive force of 5.3 (1.8) kN [18], letting the nucleus of the disc in to the cancellous bone of the vertebral body. Consequently the high pressure inside the vertebral body causes it to burst and split vertically, Figure 3.2. Under uniform axial loading, the anterior and posterior cortices fractures splitting the vertebral body horizontally [10].

Burst fracture occurs at average forces of 6.8 (2.7) kN during pure axial compression of a 3 segment thoracolumar junction [18].

3.2.2 Anterior wedge fractures

Anterior wedge fractures is characterized by a greater height loss of the anterior vertebral body, see Figure 3.3. It occurs predominantly in the T10 and L2 region of the thoracolumbar spine and is common during MVC and aircraft seat ejection maneuvers. Anterior wedge fracture affects the anterior of the vertebral body while the posterior end remains intact.

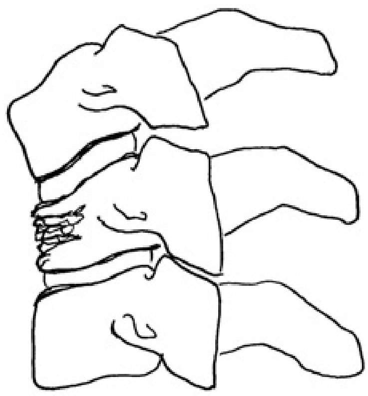

Figure 3.3: Anterior wedge fractures [Courtesy of Karin Brolin] [7]

Anterior wedge fractures are due to coupled flexion and axial compression [19]. Vertebral column is subjected to high bending strains due to the eccentricity of the center of gravity of the head and torso even during vertical acceleration leading to wedging of the anterior end [30]. Severe anterior wedge fractures involve perching of the inferior facet joint over the superior articulating joint with or without compromised intraspinous ligaments and fracturing of the spinous process and is unstable [10][35][18].

3.2.3 Lateral wedge fractures

Lateral Wedge fracture can be bilateral or unilateral. Unilateral wedge fracture involves transverse process fracture on the convex side and damage to the articular facet joints on the concave side [35]. These are unstable injuries. Lateral wedge fractures are due to bending and torsional loads. Three segment from thoracolumbar spine could tolerate an average force of 6.5(1.4) kN before sustaining anterior wedge fracture [18].

3.2.4 Dislocations and fracture disclocations

Fracture dislocations refers to the vertebral bone fracture and the dislocation of spine structures, see Figure 3.4. It differs from wedge fracture in that it involves rupture of the intraspinous process and thus the dislocation of the posterior elements. Dislocation primarily involves the facets. The facets may sustain upward subluxation, anterior dislocation with fracture or forward dislocation with locking [35].

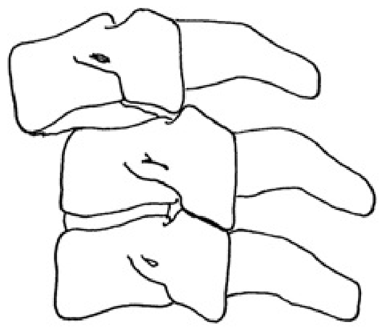

Figure 3.4: Dislocation [Courtesy of Karin Brolin] [7]

Flexion and rotation about the transverse plane or bending in the coronal plane is often the type of loading leading to dislocation injury. Fracture dislocations are clinically unstable.

3.2.5 Chance fractures

chance fractures are common type of injury caused by use of lab belts without shoulder belts. During frontal impacts the lap belt rises above ilium or the wing bones, and causes the lumbar spine to flex around it. The main cause of Chance fractures is the combined effect of flexion of the spine and distraction of the posterior elements. Under such loading conditions a marked separation of the posterior elements is observed without wedging the vertebral body or dislocating the facets. The first fracture in Chance injury start at the posterior end of the vertebral foramen and often involve splitting of the spinous process.

Neuman et al 1995 [45] reported average flexion moment of about 185 Nm before failure of lumbar FSU is sustained under dynamic flexion shear loading during simulatinig lap belt injury.

3.2.6 Hyperextension injuries

Hyperextension injury is marked by the avulsion of the superior end of a vertebrae. It is sometimes accompanied by additional injury to the posterior end of vertebral body which causes loss of vertebral body height. Moreover the articular facets, pedicles and lamina may be affected.

Hyperextension injury is hypothesized to be due to the push of mechanical forces on the torso while it is held back by a shoulder belt [19]. They are common in aircraft seat ejection maneuvers.

3.2.7 Soft tissue injuries

Herniated discs, avulsed ligaments, and fibers are classified under soft tissue injury category. Soft tissue injury usually leads to low back pain. In MVC soft tissue injury occurs, primarily, during mild rear end collisions, vehicles traversing mild speed bumps and vehicles colliding in an intersection [19].

3.3 Injury tolerance

Thoracolumbar injury tolerance depends upon loading type, spine level and number of spinal segments under test, posture of the specimen under impact and loading rate among others. Tolerance of the thoracolumbar spine model reported in literature are tabulated in this section.

Table 3.1: Thoracolumbar spine injury tolerance reported in literature

Loading type	loading rate	Specimen	Posture	Tolerance	Reference
Compression	1m/s	Lumbar FSU	Neutral	11-13KN	[54]
Compression	1m/s	T12-L5	Neutral	5-6KN	[54]
Compression	5.1m/s	T12-L2	Neutral	9.5-12KN	[29]
flexion	3.5deg/s	T12-L2; L4-S1	Neutral	140(18)Nm; 2.15(0.17)KN	[55]
anterior shear and flexion	3.5deg/s; 4mm/s	T12-L2;L4-S1	Neutral	174(58)Nm; 2KN;2KN	[55]
anterior shear and flexion	12gpeak, 15ms rise-time	lumbarFSU	Neutral	185Nm(15); 600(45);4.4KN	[44]

4

Thoracolumbar Spine Experiment

Data was collected to give an overview of the subject matter and identify relevant factors that can help shape the evaluation work. Following this a literature review was conducted to collect experimental data associated with the thoracolumbar spine having potential to validate the model. These experiments ranged from a single vertebra to intact cadavers but also ligaments, facet joint and isolated discs, and from static to dynamic loading rates and covered all kind of loading modes.

Experimental and theoretical work in the thoracolumbar spine has been carried out inspired by the occurrence of the thoracolumbar spine injuries in aircraft ejection systems. In the past few years increasing thoracolumbar fractures in MVC were identified and the experimental motivation have shifted accordingly. Experiments associated with the thoracolumbar spine can in general be classified in to those involving human volunteers, subhuman primates, human cadavers and spine segments. Since objective is to assess biofidelity only cadaveric experiments were sought. About 20 experimental data were collected, Table 4.1, however, majority of these lacked clearly defined boundary conditions and reconstruction was not possible. The data that were collected are described below grouped by spinal level tested during the experiments.

Neuman et al 1992 [43], 1995 [45], Osvalder et al 1992 [44], Demetro et al 1998 [47], 1999 [50], Duma et al 2006 [54] conducted dynamic tests on the lumbar spine. The specimens tested were FSU and intact T12-L5 specimen. These experiments had either well defined boundary conditions or was confirmed that simulation is insensitive to the missing boundary condition and the simulation could proceed. All of these experiments were reconstructed in this thesis work. Details are given in section 6.1.

Yoganandan et al 2013 [21] implemented drop tower apparatus to identify failure tolerance for segments from the entire thoracolumbar column under dynamic compression. During the test the T1-L5 spine column was cut in two three, upper thoracic (T2-T6), lower thoracic (T7-T11) and lumbar (T12-L5). Two accelerometer and two load cell were attached to the upper and lower part of the specimens and dropped from three different heights. The report however lacked clear definition of critical boundary conditions during the test. Material property of the foam padding that shapes acceleration pulse as the specimen hit the ground was not specified. Accelerometer data was not published. Unpublished data was requested to no avail. Thus it was not possible to successfully reconstruct this experiment.

Several other experiments focused on the thoracolumbar junction. Willen 1994 [29], kifune 1995 [18] were among these. The objective of these studies were to test stability of the injured thoracolumbar junction. Hence The specimens were first loaded under static flexion to establish physiological mobility, followed by dropping a ball mass from 2m above the specimen to impart injury and finally measure range of motion of the injured motion segment. Only tolerance for different type of bone fractures were reported.

On the other hand, full thoracolumbar spine experiments could help understand the behaviour of the thoracolumbar spine better than the thoracolumbar segments does. Myklebust et al 1982 [56] and Sances 1986 [57] were found in this category however they failed to report orientation of the tested specimen and simulation could not be performed.

In the category of full cadaveric experiments king and Vulcan 1971 [58], Prasad et al 1974 [30] and Luet et al 2012 [59] were reviewed. The principal result measured in the first experiment was strain of the lumbar vertebral bodies. Vertebral bodies in THUMS are Rigid and stress can not be calculated. [59] was a well defined sled test but only acceleration of the T1 and T12 vertebral bodies was reported and no information on load tolerance of the thoracolumbar injury was given. Cadaveric xperiment by Prasad et al 1974 [30] reported axial loads at the L3 or L4 vertebras during a 6g, 8g and 10g vertical accelerations. The acceleration pulse used in this experiment can not be clearly identified and the type of the shoulder harnesses used to secure the cadavers to the sled was not specified. hence reconstruction was not possible.

Several other experiments were not simulated either due to the loading mode was irrelevant [60], loading rate was static or cyclic [61][37][56][57][62][60][63][64] or the specimens tested were vertebral bodies [65]. All experiments from literature are tabulated in 4.1.

Table 4.1: Cadaveric thoracolumbar spine experiments in literature

Author, Year	# specimens	Vertebrae	loading type	Loading rate	Results
Demetropoulos 1998 [47]	10	T12-L5	(8 tests) compression, tension, flexion (ant,post,lat), shear (ant,post,lat)	100mm/s	F vs D; M vs D; Stiffness; Peak Load
Demetropoulos 1999 [50]	11	T12-L5	(3 tests) a, Flexion, b, Extension c, Extension with muscles	4m/s	M Vs Angle F Vs D (compression, shear)
Duma 2006 [54]	2 4	T12-L5 L1_2, L2_3, L3_4, L4_5	Compression to failure test	1m/s	F vs D ; M vs D
Yoganandan 2013 [21]	3	T12-L5	Compression	Drop Tower	Peak F and Peak M
Yoganandan 1994 [64]		L1-L5	cyclic flexion		
Yamamoto and Panjabi 1988 [66]	10	L1-Sacrum	Flxn, Extn, Rot (L and R) Lat Bending (L and R) M (2.5Nm-10Nm)	Static	NZ, EZ, ROM for each Vert in L1-S
Belwadi and yang 2008 [55]	19	L3-T12 and,S1-L4	(2 tests) i, Ant shear-flexion ii, flexion only	3.5deg/sec flex and 4mm/sec shear	compression, shear, flexion
Neuman 1995 [45]	20	level of specimens L1-L2 L3-L4	(3 consecutive. loadings) a, static (fxn-shear25Nm,100N) b, dynamic (flexion, flexion-shear) c, a, static (fxn-shear25Nm,100N)	pendlum (250mm above the mid disc plane)	shear, tension, flexion M vs D flexion angle, vert and horz D
Schendel 1993 [63]	5	L1-L2	flexion,extension,torsion	Static	F_{facet} vs M_{ext}; F_{facet} vs M_{lat} F_{ALL} vs M_{ext} ; F_{ALL} vs M_{flx} F_{facet} vs Rot ; Rot vs flex/ext
Garges 2008 [60]	15 15	L2-L3 L4_L5	torsion	1deg/sec 5deg/sec	D, Stiffness, Torque, Energy
Begeman 1994 [61]	1 1 9 5	L1-L2 L2-L3 L3-L4 L4-L5	(2 tests) i, Quasi static loading() ii, Dynamic loading	0.5-50mm/s	Static Stiffness Dynamic Stiffness
Yoganandan 1988 [65]	63	T12-L5, vertebral body	Compression	2.5mm/s	Failure load for each level
Myklebust 1983 [56]	3,1,4	T3-L5, T2-L5, T3-S	Compressive force	1-120cm/sec	Failure level, Force, angle "
Sancez 1986 [57]	29	18, T3-L5 6, spines	compression-flexion	1cm/sec	Failure level, load, angle Mmax
Kifune [18] 1995	10	T11-L1	a, Dynamic Compression b, Static flex, ext, lat bend (L&R), axial Rot (L&R)	Drop ball (5.2 m/s)	NZ,EZ,ROM for Intact, Endplate, Wedge and Burst fractures
Willen 1984 [29]	7(age $<$ 40)	T12-L2	a, dynamic Compr(drop ball) b, static compr, tension,fxn, extn	Drop ball (6.3 m/s)	Δ Diameter in V.body, spinal canal, b, $F_{failure}$ Vs time in (a)
Langrana 2002 [37]	3,3,1,2	T12-L2, T10-T12, T11-L1, T8-T10, T10-T12	i, 15deg ext, compression, ii, neutral, compression iii, neutral, compression no post elem	$100mm/s$	$F_{failure}$, Strain at 75% $F_{failure}$, Stiffness
Stemper 2010 [62]	48(age $<$ 40)	T4.-T5, T6.-T7, T8-T9, T10-T11	a, Compression b, Tension	Static	Stiffness, E
Pintar 1992 [67]	38cadavers 132 ligaments	all ligaments except ITL	Tension		Stiffness, Strain, Length, F vs D, Crossection Area
Myklebust 1983 [56]	12	Ligaments (All,PLL,LF,ISL,CL)	Axial Tension	1 to 100cm/s	$F_{disruption}$
Myklebust 1983 [56]	4	intact Cadavers	Compression	1cm/sec	Failure level, Force, angle
King and Vulcan 1970 [58]		PHMS	Sled test		Strain at L3, L4
Luet 2012 [59]		PMHS	sled test	acceleration pulse	T1 and T12 acceleration
Prasad 1974 [30]		PMHS	sled test	acceleration pulse	Load at L3 acceleration

5 Methodology

In this chapter details of the procedures that were followed are summarized. The experiments and their reconstruction are laid down and challenges in simulation and how they were overcome are stated. Previous validation works on THUMS cervical spine and other thoracolumbar models are addressed followed by a brief description on the simulation of the Global Human Body Model Concertium GHBMC model. Two intervetebral discs material models in literature are also presented.

5.1 Selection of experiments

About 20 experiments on the thoracolumbar spine were found in literature. Many of these experiments were static or lacked critical setup details. Therefore only four experiments, [54][50][44][55], were selected to evaluate the model. Selection of the relevant experiments was carried out by an extended research group with members from Vehicle and Traffic Safety Center at Chalmers (SAFER), Volvo Cars Corporation and Sahlegrenska university hospital. Selection was in general based on loading rate, loading type and spinal level tested in the experiments. Dynamic experiments which exceeds 0.6 m/s, were prioritized to mimick MVCs [6].

5.2 THUMS

THUMS is FE-human body model for vehicle safety. It represents 50th percentile American male (175 cm tall and weighing 77 kg) in a sitted occupant posture. THUMS was first developed in 1997 by Toyota Central R&D Labs and Toyota Motor Company in conjunction with Wayne State University [68]. It has been validated against 35 cadaveric and volunteer tests in frontal, rear and lateral impacts. It is now used by more than 20 vehicle industries and research institutes [69].

The thoracolumbar spine of THUMS version 1.4 and 3.0 are identical. Autoliv Research have modified and improved the thorax and chest of THUMS version 1.4 [24][25], but the thoracolumbar spine was not modified. The work in this project is based on the thoracolumbar spine model for all three versions, hereafter referred to as THUMS thoracolumbar model.

The thoracolubmar spine model in THUMS is a long structure of solid, shell and seatbelt elements. It consist of about 16,825 elements in total. All vertebral bones in the thoracolumbar spine model are modelled as rigid bodies (mat20). Each vertebral bone in turn consists of shell and solid elements for the cortical and spongy bones respectively. Both the upper and the lower endplates are made up of inner solid elements as the cartilagenous bones and outer rigid solid elements as the vertebral bone.

The nucleus and the annulus fibrosus of the intervertebral discs are modelled as elastic material (mat001). The annulus fibrosus is further classified in to outer and inner parts differing in Young's modulus. Similarly, fibers of the discs are modelled as tension only seat belt elements (matB01).

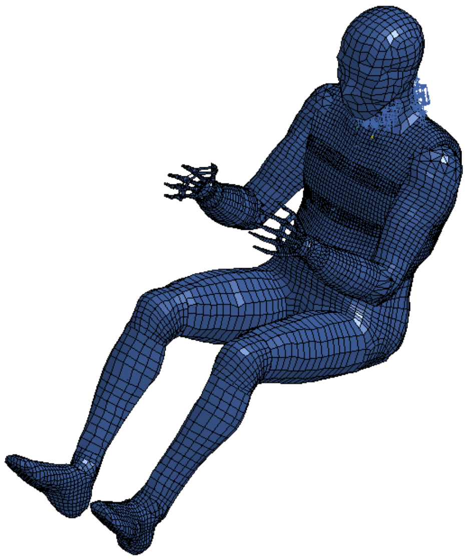

(a) THUMS

(b) Thoracolumbar spine model in THUMS

Figure 5.1: THUMS and Thoracolumbar spine model in THUMS

The cortical bone, spongy bone and the endplates, with in a single vertebral bone, are rigidly constrained to one another. Automatic surface to surface contact is defined between two adjacent vertebral bones throughout the spinal column. Stiffness of the ligaments is specified via two force versus strain loading and unloading curves. The end plates and the discs share the same nodes. Likewise, nodes are shared by the ligaments and the vertebral bones at the point of attachment.

5.3 Simulations

Experiments were reconstructed in LS-PrePost (versions 4.1 and 4.3 Beta, Livermore Software Technology Corporation, Livermore, CA) and run with an explicit dynamic solver (LS-DYNA version 9.71, Livermore Software Technology Corporation, Livermore, CA). LS-PrePost (versions 4.1 and 4.3 Beta, Livermore Software Technology Corporation, Livermore, CA) and Matlab R2015b (The MathWorks Inc., Natick, MA, 2015) were used for the Post-processing tasks.

Simulation matrix of the four experiments and one ligament test [67] is given in Table 5.1. Reconstruction of these experiments is described in the following sections.

Table 5.1: Test Matrix : contacts = intervertebral contact

		Exp 1 (sec: 5.3.1)		Exp 2 (sec: 5.3.2)		Exp 3 (sec: 5.3.3)	Exp 4 (sec: 5.3.4)		Exp 5 (sec: 5.3.5)
		FSU	T12-L5	Flex	Ext		Flex-Shear	Flex	
THUMS (sec: 5.2)	Contacts	x	x	x	x	x	x	x	x
	No Contacts	x	x	x	x	x	x	x	
Disc-1 (sec: 5.4)	Contacts	x	x	x	x				
	No Contacts	x	x	x	x				
Disc-2 (sec: 5.4)	Contacts	x	x	x	x				
	No Contacts	x	x	x	x				
GHBMC (sec: 5.5)		x	x	x	x				

5.3.1 Dynamic compression test

Duma et al 2006 [54] conducted lumbar spine tests. Objective of the study was to determine biomechanical property of the lumbar spine under dynamic compression loading.

Two T12-L5 segments and Four lumbar FSUs were axially compressed at 1 m/s using electrohydraulic material testing machine, figure 5.2. One half of superior and inferior vertebrae were placed in a bonding compound in custom made potting cups. The inferior end of the inferior vertebra (L5) was at an angle of 18° with the horizontal. A six axis load cell situated at the lower end of the setup was used measured reaction force and moment. Specimens were further equipped with two accelerometers and a high rate video was recorded for motion analysis but the results were not published. In all the FSUs, the superior end plate of the inferior vertebra were fractured at loads from 11,203 kN to 13,065 kN. The two T12-L5 segments sustained compression fractures at 5,009 N and 5,911 N axial force and 250 Nm and 300 Nm bending moment respectively. No sign of buckling was observed in the FSUs.

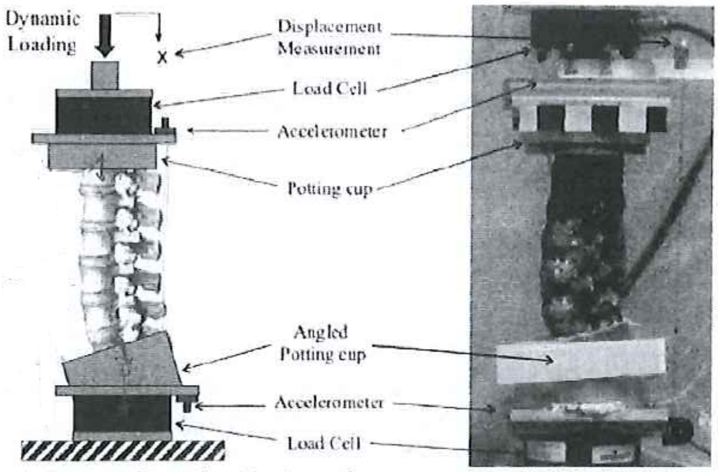

Figure 5.2: Compression test setup [54]

Models T12-L5 and L1-L2, L2-L3, L3-L4, and L4-L5 segments including corresponding ligaments and intervertebral discs were used. The upper and the lower potting were modelled as cylindrical rigid bodies ($\rho = 1.420e^{-6}$ kg/mm^3, E =3.0GPa,$v = 0.4$), Figure 5.3. The potting were rigidly constrained to their adjacent vertebrae. The lower potting was fixed in space while the upper potting was prescribed 1 m/s velocity, see Figure 5.4, in the vertical direction to compress the specimen.

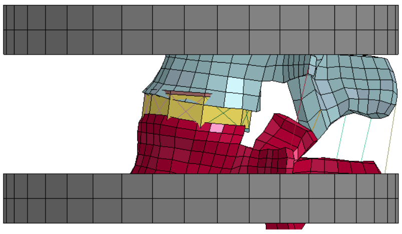

(a) FSU

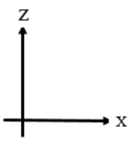

(b) Global axis

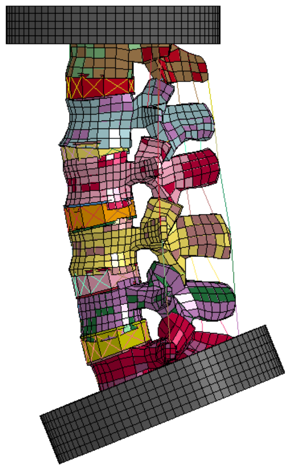

(c) T12-L5

Figure 5.3: Reconstruction of the compression test in Section 5.3.1

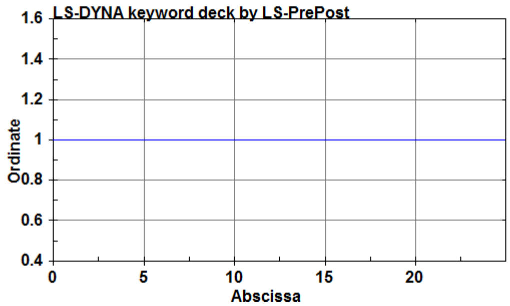

Figure 5.4: Load curve used in simulating Section 5.3.1 ordinate = Force (kN), abscissa = time (msec)

Horizontal offset between the upper and lower potting during the experiment was not specified. Therefore, sensitivity test was carried out with 4 mm, 10 mm, 12 mm and 14 mm horizontal offsets. These offsets were introduced by pulling the inferior end posteriorly relative to the superior end during model positioning.

5.3.2 Dynamic flexion and extension tests

This experiment was conducted by Demetropoulos et al 1999 [50] to establish stiffness of lumbar spine under dynamic flexion and extension moments prescribed at 4 m/s.

The T12-L5 specimen was positioned upside down and potted in an aluminum cup weighing 1.6 kg, see Figure 5.5. Potted specimen was then mounted on an Instron servo-hydraulic material testing machine via a five axis load cell which inturn was connected to L-shaped fixture via an angled bracket. The L shaped fixture keept the specimen perpendicular to the testing machine and the angled bracket with adjustable angle and orientation accounted for the pelvic angle in a seated occupant. The inferior end of the specimen hung freely under the influence of gravity. 800 mm long steel cable transferred the translational force from a DC-motor to the lower end of the specimen. The specimen were prescribed at 4 m/s.

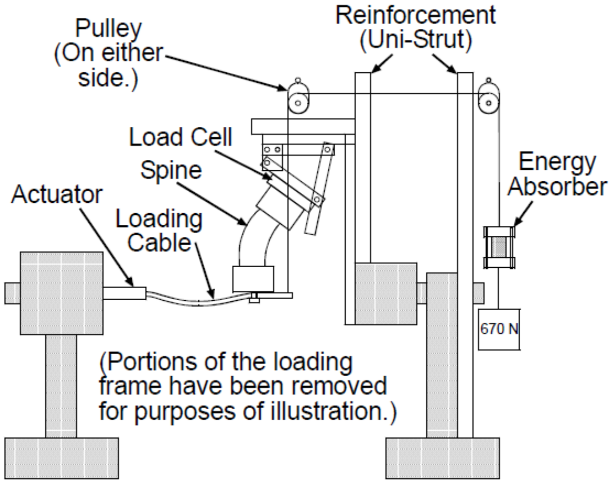

Figure 5.5: Dynamic flexion and extension tests setup [50]

T12-L5 model including the ligaments and intervertebral discs were used. A cylindrical rigid body ($\rho = 6.048e^{-6}$ kg/mm^3, E =69.0GPa,$\upsilon = 0.3$) was used to model the lower potting, see figure 5.6. The total mass of this potting was 1.61 kg according to the experimental data. L5 vertebra was fixed in space and 800 mm long single element beam (E= 2000 GPa) was used to mimick the steel cable.

To study influence of different postures, two orientations, see Figure 5.6, based on the diagram reported for the experiment, were simulated and compared. The main difference between the two postures was the curvature. One had very large curvature, figure 5.6b until initial penetration was closely approached and the other had a relatively smaller curvature, see figure 5.6a. Large curvature posture was obtained by fixing the lower four vertebrae and applying shear and flexion magnitude to the superior end. Care was taken to keep aspect ratio of the disc elements to less than half and to avoid initial penetrations. similarly, for the smaller curvature posture, the superior end was prescribed to translate and rotate simultaneously while the three most inferior vertebrae were fixed. The ratio of the translating to rotating curve was 5 to 1 in the larger curvature posture and 2 to 1 in the smaller curvature posture, the smaller load curve is shown in figure 5.4, in the previous Section, and the others are scaled version of this figure. The main loading curve used for simulating the experiment is given in Figure 5.7.

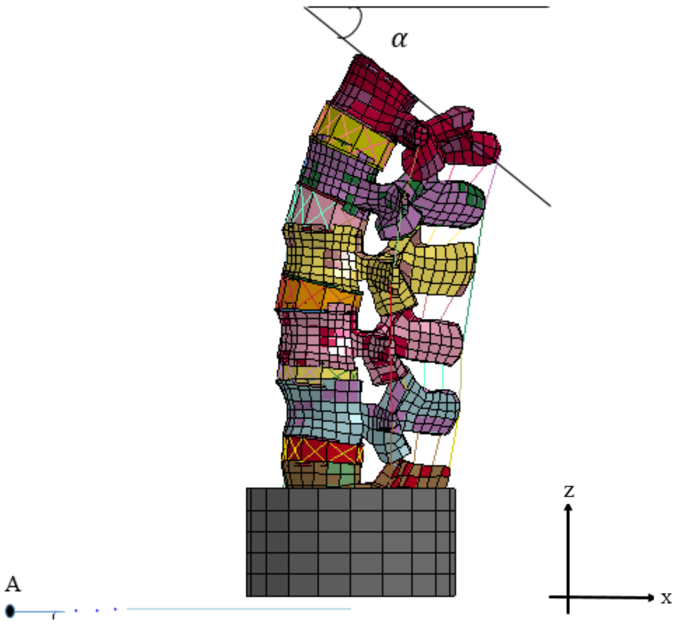

(a) posture-1: small curvature

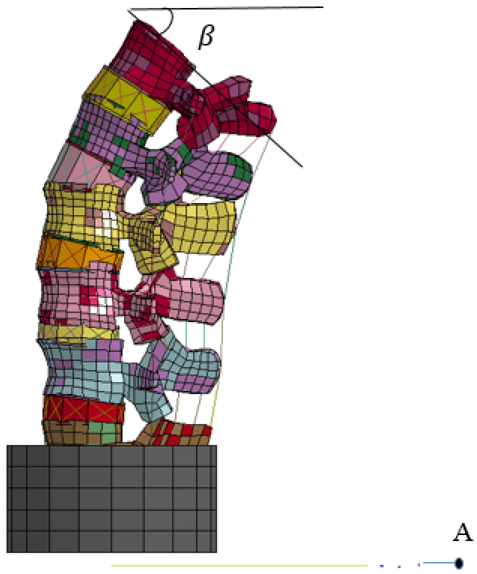

(b) Posture-2: Large curvature

Figure 5.6: Reconstruction of the dynamic flexion and shear tests in Section 5.3.2: postures used for sensitivity test and global axis: $\alpha = 25°$, $\beta = 30°$, A = point of application of displacement

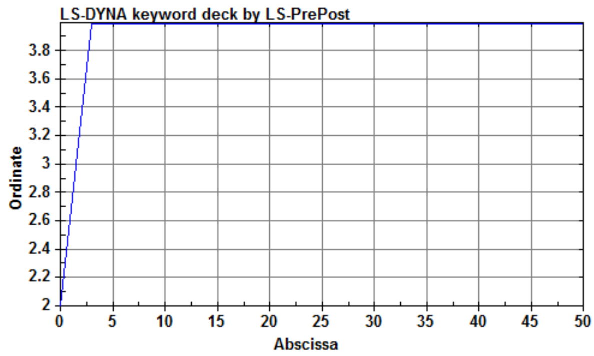

Figure 5.7: Load curve used in Section 5.3.2 Showing ramping for the first three msec; ordinate = Force (kN), abscissa = time (msec)

The reported parameters (vertical and horizontal length of specimens) were roughly about 90% recreated. This is believed to be the best possible considering that mobility of the model (without penetration) is very limited and the complementary nature of these parameters. Reaction force and moment were extracted at the superior end whereas angular displacement was taken at the inferior end.

5.3.3 Dynamic shear and flexion test

Four experiments were conducted by Neumman et al 1992, 1995 [43][45] and Osvalder et al 1990 [70], 1993 [44] to identify flexion-distraction injury mechanisms and tolerance levels resulting from the use of lap belts in frontal crashes.

The main reference article here was [44] but data was also taken from the other experiments. Twenty L1-L2 and L2-L3 FSUs were loaded in three stages: static flexion and shear, dynamic flexion and shear and static flexion and shear. The first static loading served to determine physiological mobility and to precondition the specimens. The dynamic flexion-shear loading test was used to study the dynamic response and to impart injury. The final static loading was used to determine mobility of the injured lumbar FSUs. Only the dynamic part of [44] was simulated in this thesis.

The FSUs were potted in steel cups with plastic adhesive and stainless steel screws to secure the setting. The lower end plate of the intervertebral disc was parallel to the superior end of the lower potting cup [70].

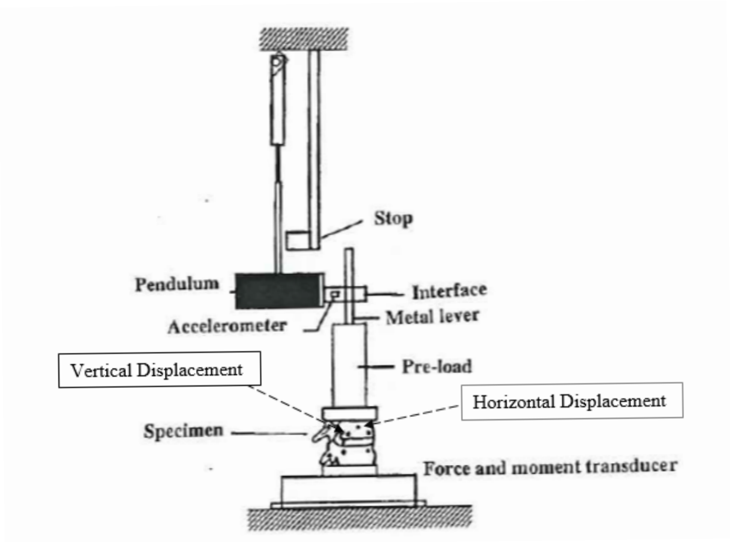

Figure 5.8: Dynamic flexion and shear test setup [44][45]

Setup of the dynamic test is shown in figure 5.8. A 12 kg preload was fixed on the top of the upper potting centered about posterior end of the vertebral bone as deducted from the reported setup diagram. A metal interface was fixed above the torso mass. A padded pendulum strikes the metal interface 250 mm above the mid-disc plane. A stop prevented the pendulum from imparting further loading than required. A load cell was placed between the specimen and the ground and a linear accelerometer on the metal interface.

Three group of ten specimens each was subjected to three different acceleration pulses. The first pulses had a peak of 5g after 30 ms, the second pulse had 12g after 15 ms and the third pulse a peak of 12g after 5 ms. Reaction moment, shear force and horizontal, vertical displacements were reported. Horizontal displacements were taken at mid level of the upper vertebral body while vertical displacements were measured at the mid posterior end of the vertebral body [45].

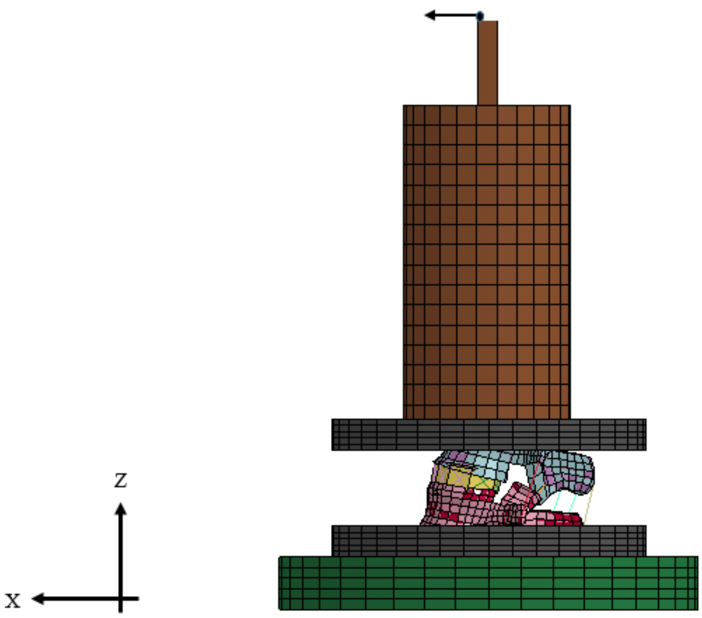

Figure 5.9: Reconstruction of the dynamic flexion and shear test in Section 5.3.3 and global axis: arrow points direction and postion of application of acceleration pulse

The L1-L2 and L2-L3 models with intervertebral discs and ligaments intact were used. The vertebrae were rigidly merged to the solid aluminum potting ($\rho = 6.048e^{-6}$ kg/mm^3, E =69.0GPa,$v = 0.3$), see figure 5.9. The torso mass was modelled as a rigid cylinder, 150 mm high and 80 mm in diameter, with a mass of 1.6 kg. The metal bar, torso mass and the upper potting were constrained to one another.

The lower potting was fixed in space while linear acceleration was prescribed using two of the three acceleration pulses defined in [44], see figure 5.10. Acceleration pulse was zero for the first 20 msec in all experiments to allow the torso mass to fully load the model before the test was started. Reaction forces and moments were measured at the lower potting. Flexion angle was defined as the angle between the upper potting and the lower potting. Horizontal and vertical displacement were recorded for two different locations (corresponding to the experiment) on the upper vertebrae.

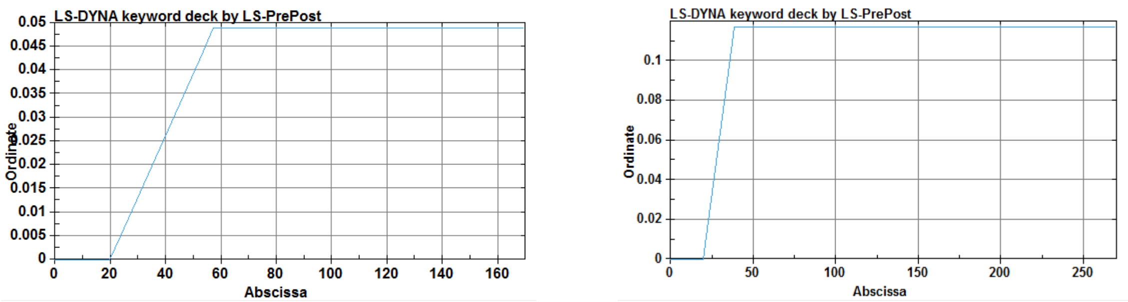

(a) Moderate Pulse

(b) Severe Pulse

Figure 5.10: Acceleration pulses used in Section 5.3.3: oridinate = g (0.00981 mm/msec^2), abscissa = time (msec)

5.3.4 Static flexion and shear and flexion only tests

Belwadi and K. Yang [55] conducted in vitro experiment on lumbar motion segments under coupled static flexion and shear and flexion only loading. The main aim of the study was to investigate injury mechanics and tolerance of lumbar cadaveric motion segments.

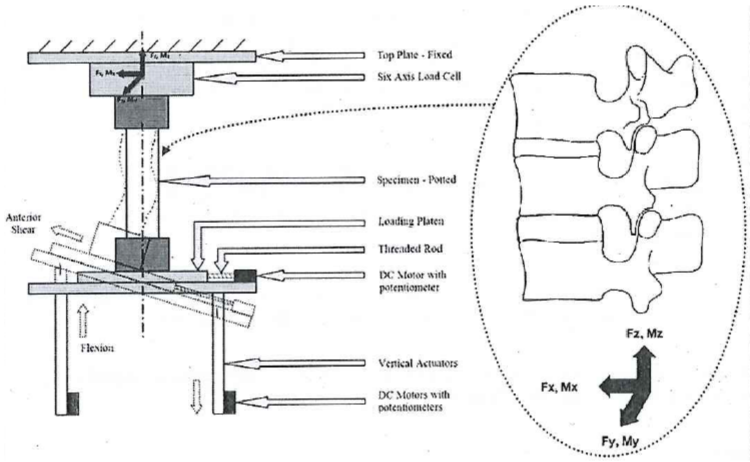

Figure 5.11: Static flexion and shear and flexion only tests setup [55]

The set up can be seen in fig 5.11. Motion segment T12-L2 and L4-S1 were positioned up side down and potted in aluminum cups at both ends. Care was taken to ensure that the superior end plate of the T12 and L4 vertebra were parallel with the superior end of the inferior potting. A DC-motor mounted on the test set up imparted shear force on the inferior potting at 4 mm/s while the superior end was fixed. Flexion was applied via two opposite coplanar forces at 8 mm/s acting at the two edges of a 256 mm wide platan. This is equivalent to 3.6°/sec (= 0.061rad/sec) of flexion moment.

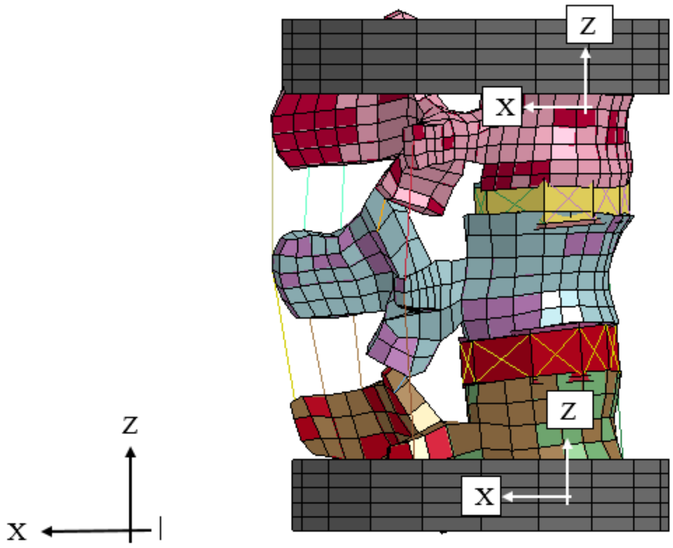

Figure 5.12: Reconstruction of the static flexion and shear and flexion only tests in Section 5.3.4 and the global and local axes for load cell beam element and the shear loading

The T12-L2 model including discs and ligaments were used. The model was carefully set up according to the experimental specifications, see figure 5.12. The lower and upper potting were modeled as rigid material ($\rho = 2.70e^{-6}$ kg/mm^3,E= $68.9GPa$,$v = 0.33$). Flexion was prescribed in local coordinate system while anterior shear in the global coordinate system. A linear elastic discrete beam element (TKR ,TKS, TKT = $1.0e^{-3}$ and RKR, RKS, RKT = $1.0e^{-6}$) was added between the upper vertebra and its potting to measure forces and moments. Loading curves used in this simulation are provided in Figure 5.13.

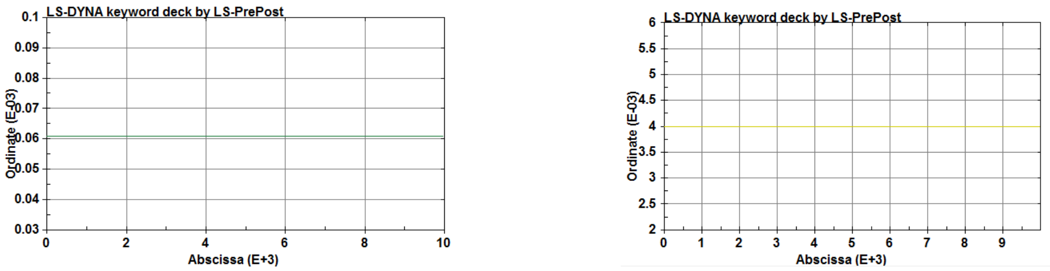

(a) Flexion

(b) Shear

Figure 5.13: Load curves for flexion and shear loading in Section 5.3.4: ordinate = velocity (m/s in shear and rad/sec in flexion), abscissa = time (msec)

5.3.5 Ligaments test

Pintar et al 1992 [67] conducted a test on lumbar spine ligament to determine biomechanical properties for direct incorporation in to mathematical human body models. The specimen included 38 human cadaveric samples from all spinal ligaments except the ITL. Initial length and crossectional area of the ligaments were obtained using cryomicrotomy procedure. Stress, strain, stiffness in N/mm and energy at failure were reported for each ligament type.

Strength of the seat belt ligaments in THUMS is specified via two force versus strain loading and unloading curves, see figure 5.14. Length of each ligament was measured and multiplied by the strain (abscissa) of the loading curve (according to equations (5.1)) to obtain Force versus deformation curve from which stiffness was calculated for each ligament type (according to equation (5.2)). The average stiffness and the average length for the same ligament type were then compared against the reported average ligament stiffness and lengths in [67].

$$\varepsilon = \frac{\Delta L}{L} \tag{5.1}$$

$$K = \frac{F}{x} \tag{5.2}$$

where ε = Engineering strain, ΔL = change in length, L = initial length, K= stiffness, F= force, x = deflection

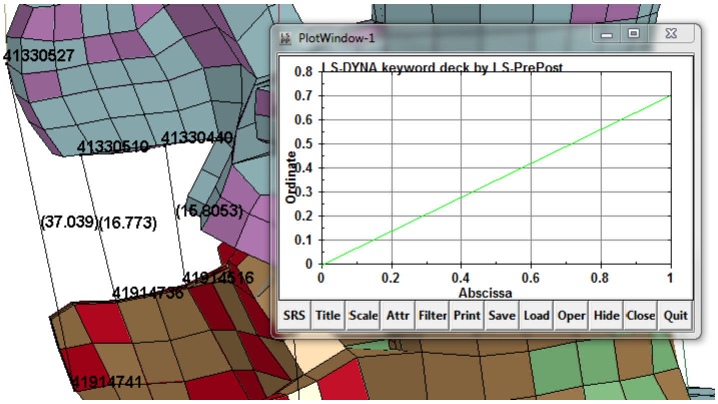

Figure 5.14: Sample length (mm) and Force (kN) versus strain curve for ligaments in THUMS

5.4 Modified intervertebral disc models

It was thought that testing additional disc models in THUMS could help better understand the response but might also correct certain weaknesses that were observed in THUMS. Two additional material models for the disc are collected from literature and are used to simulate the first two experiments, [54][50] (see also Sections 5.3.1 and 5.3.2) and the results were compared with the response of THUMS.

The first simple intervertebral disc model had the same material model as THUMS but higher Young's modulus. It was adapted from the comprehensive literature review on lumbar spine discs conducted by Kurutz et al [26], Table 5.2. This disc will be referred to as disc-1 henceforth.

Table 5.2: Intervertebral disc material model [26], disc-1

	Material type	R.O.(Kg/mm^3)	E(GPa)	υ	Reference
Nucleus pulposus	Linear Elastic,isotropic	1.0e-06	0.001	0.499	[26]
Annulus ground substance	Linear Elastic, isotropic	1.0e-06	0.004	0.4	[26]
Annulus fibers	Tension only Elastic Fibers	-	500	0.3	[26]

The second material model was taken from the cervical spine's disc model compiled by Östh [71]. The nucleus pulposus was modelled as viscoelastic and was originally obtained from Panzer et al [72]. Similarly Hill-Foam material model was used to represent the ground substance of the annulus fibrosus according to Iatrides et al 1996 [73]. Some parameters of the disc model are in Table 5.3, details are given in appendix A.5: simulation Cards, Material models for discs. It should be mentioned here that majority of the references during fitting the models was taken from lumbar spine's data hence this disc model could be equally applicable to the lumbar spine. Details for this material model are found in [71]. This disc will be referred to as disc-2 henceforth.

Table 5.3: Intervertebral disc material model [71], disc-2

	Mat	Sec	R.O.(Kg/mm^3)	Bulk/K (kN/mm^{-1})	Ref
Nucleus	Viscoelastic	solid	1.0e^{-6}	1.72	[71]
Annulus ground substance	Hill-Foam	solid	1.0e^{-6}	3.38	[71]

5.5 Evaluation of the GHBMC model

The lumbar spine model of the Global Human Body Model Concertium model GHBMC was also evaluated in this thesis work against the same two experiments, [54][50] that were used to evaluate THUMS, see table 5.1. The GHBMC has been evaluated under flexion test in full body model [3]. In this thesis the lumbar spine (T12-L5) was isolated and tested under the dynamic compression test [54] and the dynamic flexion and extension tests [50].

The same procedures were adapted for GHBMC as for THUMS during reconstruction as described in Sections 5.3.1 and 5.3.2.

Figure 5.15: The GHBMC model [3]

6

Results

In this chapter simulation results to the experiments described in sections 5.3.1, 5.3.2, 5.3.3, 5.3.4, 5.3.5 and 5.5 are given in sections 6.1, 6.2, 6.3, 6.4, 6.5 and 6.6 respectively.

6.1 Dynamic compression test

6.1.1 FSU

All four of the lumbar FSU specimens tested in this experiment failed at about 2 mm vertical deformation for 11-13 kN compressive force. For THUMS this corresponded to 2.74-4.4 kN at 2 mm deflection as in the experiment. The nature of the responses are the same but the lumbar FSU models were less stiffer than the cadaveric lumbar FSUs by a factor of three to four, Figure 6.1.

Another observation was the large dip occurring in the L4-L5 FSU, Figure 6.1. This is due to intervertebral contact force starting early. The initial separation between the two vertebral bodies is about half of the discs' height reported in [26] see Figure 6.2a. The dip is due to a sudden and momentary fall of intervertebral contact at that point in time, Figure 6.2b.

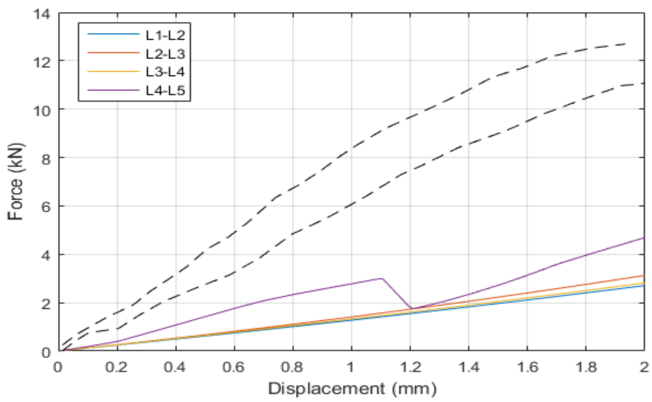

Figure 6.1: Force vs displacement response in THUMS ALR (L1-L2 = blue, L2-L3 = green, L3-L4 = red, L4-L5 = magenta) and the experimental corridor [54] (dashed lines)

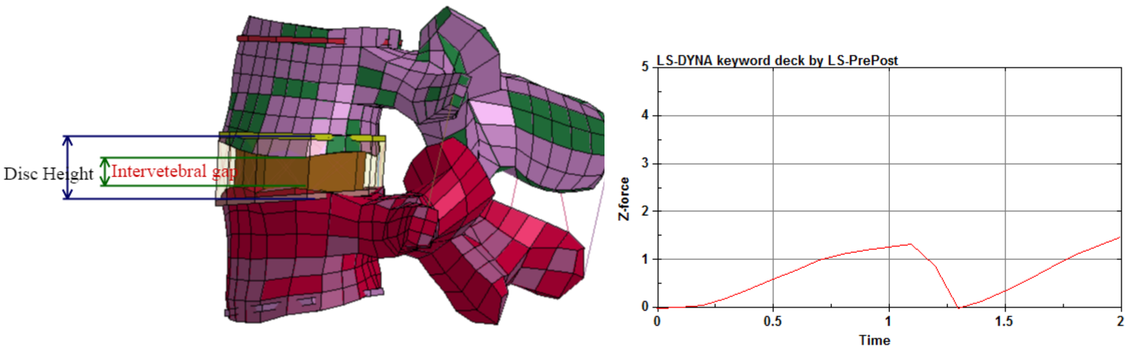

(a) **(b)**

Figure 6.2: The L4-L5 intervertebral gap (left) and the contact force (right) during simulation

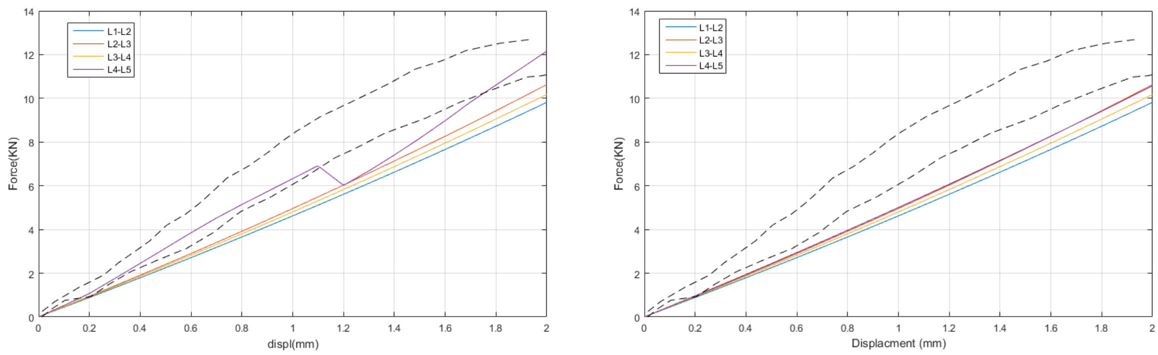

(a) **(b)**

Figure 6.3: Force vs displacement response with(a) and without(b) intervertebral contacts in THUMS (L1-L2 = blue, L2-L3 = green, L3-L4 = red, L4-L5 = magenta) using disc-1 and the experimental corridor [54] (dashed lines)

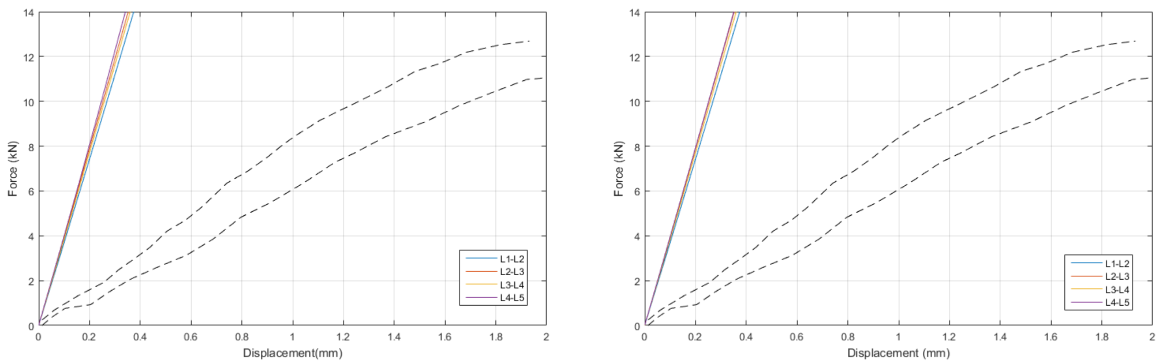

(a) **(b)**

Figure 6.4: Force vs displacement response with(a) and without(b) intervertebral contacts in THUMS (L1-L2 = blue, L2-L3 = green, L3-L4 = red, L4-L5 = magenta) using disc-2 and the experimental corridor [54] (dashed lines)

For the first simple modification made to THUMS' discs, disc-1, the response was improved considerably, see Figure 6.3a. THUMS now approaches the corridor and is only 16% off as compared to 50%-75% in the original THUMS. It can also be observed that the dip in the L4-L5 FSU persists. When the models were simulated without the intervertebral contact the L4-L5 force-displacement response became similar to the L1-L4 FSU, that is the dip was eliminated, see Figure 6.3b.

For the second simple modification made to THUMS' discs, disc-2, the response was too stiff under the dynamic compressive test, see Figure 6.4. Around 70 kN was required to compress the discs by 2mm. No notable difference could be observed for simulation with and without intervetebral contacts for this disc model, see Figures 6.4a and 6.4b.

6.1.2 T12-L5 segment

In this simulation response of T12-L5 model in THUMS was compared with its cadaveric counterpart from experimental data [54]. Sensitivity test disclosed that the response was insensitive to the tested horizontal offsets. Only activation time of the intervertebral contact was affected. The greater the offset the more activation of the intervertebral contact was delayed. The results for the 14 mm horizontal offset are presented here.

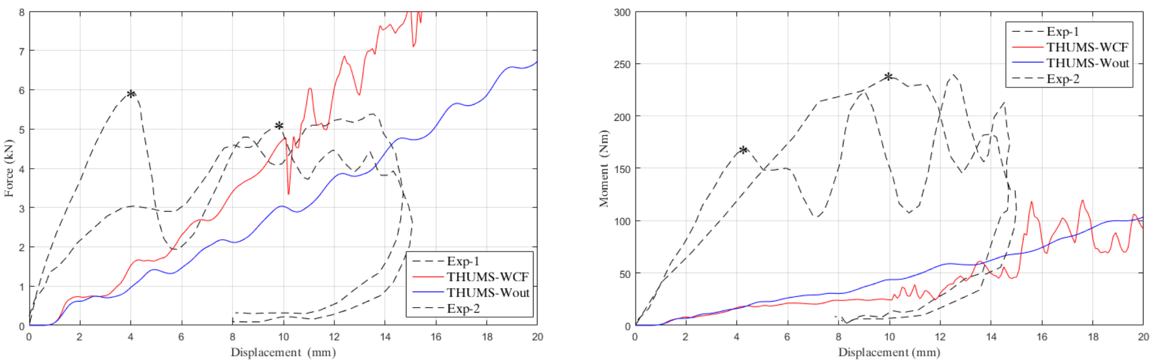

(a) Force Vs Vertical Deformation

(b) Moment Vs Vertical Deformation

Figure 6.5: Load vs displacement response of the T12-L5 model in THUMS under dynamic compression test [54]: with(red) and without (blue) intervertebral contact

Both of the cadaveric specimens in the experiment failed at about 4 mm and 10 mm vertical deformation for 5 kN and 6 kN of axial forces, Figure 6.5a. THUMS reaction force ranged from 3.3 to 4.8 kN at the same deformation. Like wise peak extension moment of 28 and 55 Nm was registered for THUMS while for the cadaveric specimens 168 and 236 Nm of flexion moment was reported for the same deformation. Reaction force of THUMS in pure compression is 20-34% less than the experiment whereas reaction moment is roughly 25% of that reported in the experiment. The large difference between THUMS response and the experiment could be due to inappropriate disc's material model, ligaments and/or intervertebral contacts.

A sharp momentary decrease in compression force at about 10mm of deflection can be seen in Figure 6.5a. This is due to the sudden decrease in contact force resulting from a change in kinematics of the column under test. In the abscence of the intervetebral contacts the column tended to buckle, see Figure 6.7c which is characterized by a decrease in reaction force and increase in reaction moment as shown in Figure 6.5. The dynamics of the model during simulation are captured in Figures 6.6 and 6.7.

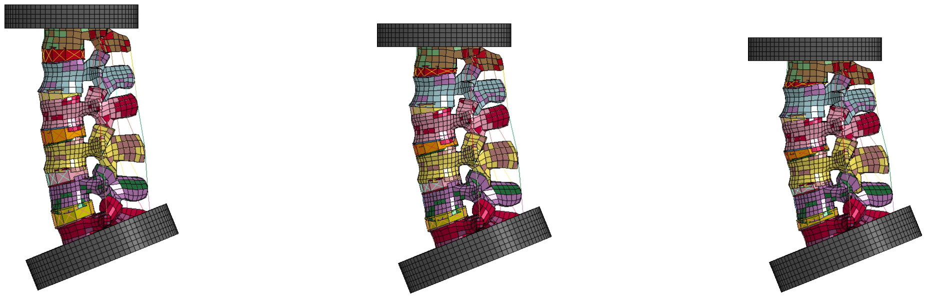

(a) 0 ms **(b)** 12.5 ms **(c)** 25 ms

Figure 6.6: Simulation of the T12-L5 model in THUMS with intervertebaral contact under dynamic compression test in Section 5.3.1

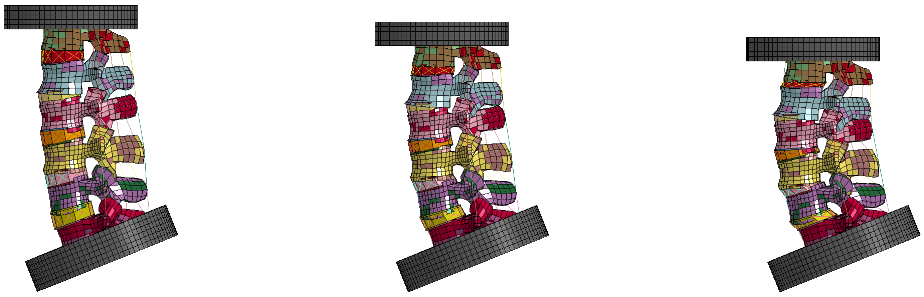

(a) 0 ms **(b)** 12.5 ms **(c)** 25 ms

Figure 6.7: Simulation of the T12-L5 model in THUMS without intervertebaral contact under dynamic compression test in Section 5.3.1

Response of the model with disc-1 is given in fig 6.8. With this disc model vibrations occurred later in time but the model's reaction force and moment misses experimental data by a relatively larger amount as compared to the THUMS in Figure 6.5. In the abscence of the intervetebral contacts the model with disc-1 tended to buckle, fig 6.10c. As a result a slightly lower reaction force and slightly higher reaction moment was obtained than for THUMS in Figure 6.5, further deviating from the experimental result. The ligaments (mostly the CL ligament) carried large forces when the model buckled and the intervertebral discs experienced relatively lower stress. The dynamics of the model during simulation are shown in 6.9 and 6.10.

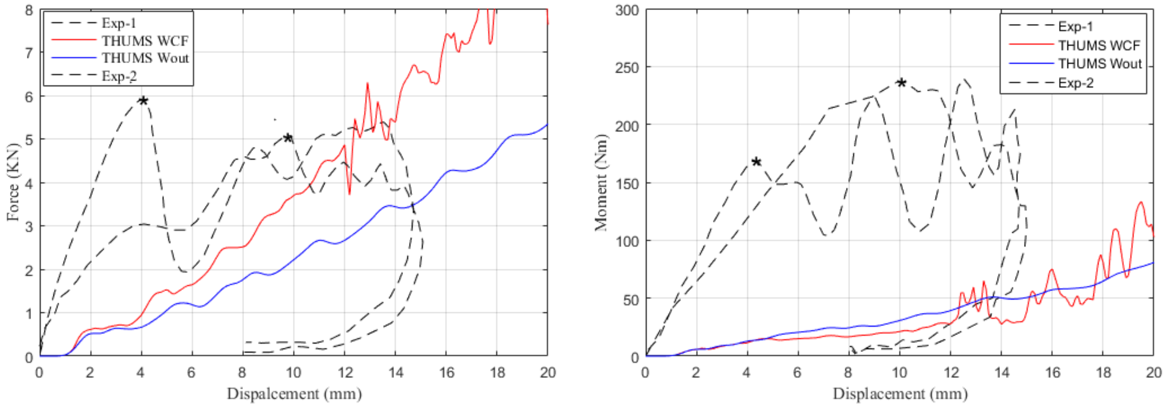

(a) Force Vs Vertical Deformation **(b)** Moment Vs Vertical Deformation

Figure 6.8: Load vs displacement response of the T12-L5 model in THUMS with disc-1 under dynamic compression test [54] : with(red) and without (blue) intervertebral contact

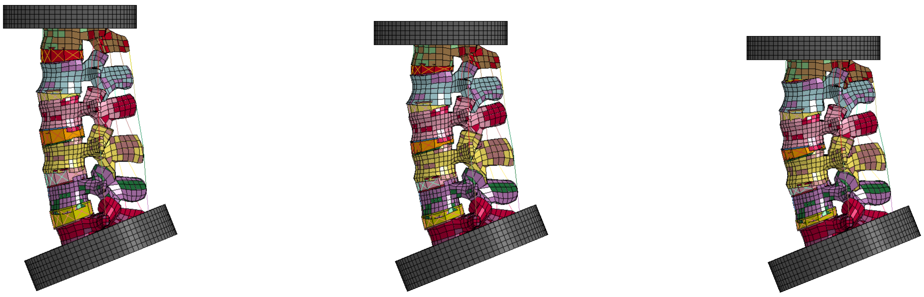

(a) 0 ms **(b)** 12.5 ms **(c)** 25 ms

Figure 6.9: Simulation of the T12-L5 model in THUMS with disc-1 and intervertebaral contact under dynamic compression test in Section 5.3.1

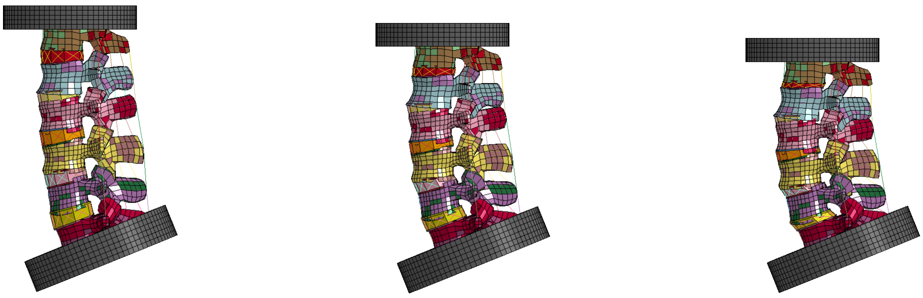

(a) 0 ms **(b)** 12.5 ms **(c)** 25 ms

Figure 6.10: Simulation of the T12-L5 model in THUMS with disc-1 and without intervertebaral contact under dynamic compression test in Section 5.3.1

Response of the T12-L5 model in THUMS with disc-2 was found to be overly stiff in compression, see Figure 6.11. No notable difference is observed in the response with and without intervertebral contacts and buckling was notable even for the simulation with intervertebral contacts, fig 6.12. This could be due to the higher stiffness of the discs and the initial inclination of the model's posture making it easier to buckle than to deform vertically. Once the specimen was in buckling mode the the CL ligament carried larger portion of the total compressive load (each CL ligament carried 1.5 kN - 2 kN force).

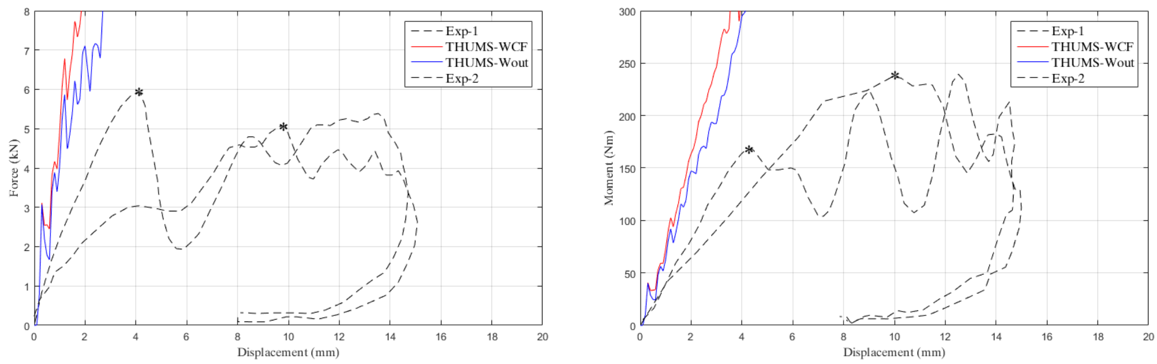

(a) Force Vs Vertical Deformation **(b)** Moment Vs Vertical Deformation

Figure 6.11: Load vs displacement response of the T12-L5 model in THUMS with disc-2 under dynamic compression test [54]: with(red) and without (blue) intervertebral contact

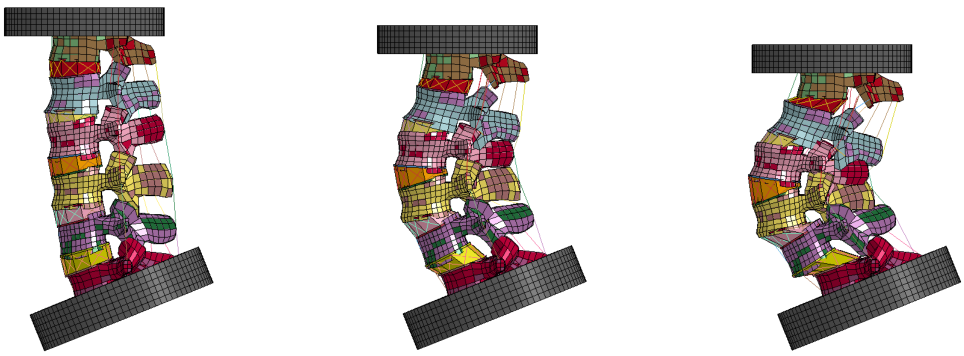

(a) 0 ms **(b)** 12.5 ms **(c)** 25 ms

Figure 6.12: Simulation of the T12-L5 model in THUMS with disc-2 and with intervertebaral contact under compression test in Section 5.3.1

6.2 Dynamic flexion and extension tests

In this experiment T12-L5 specimen was tested under dynamic flexion and extension loads. The results are given below.

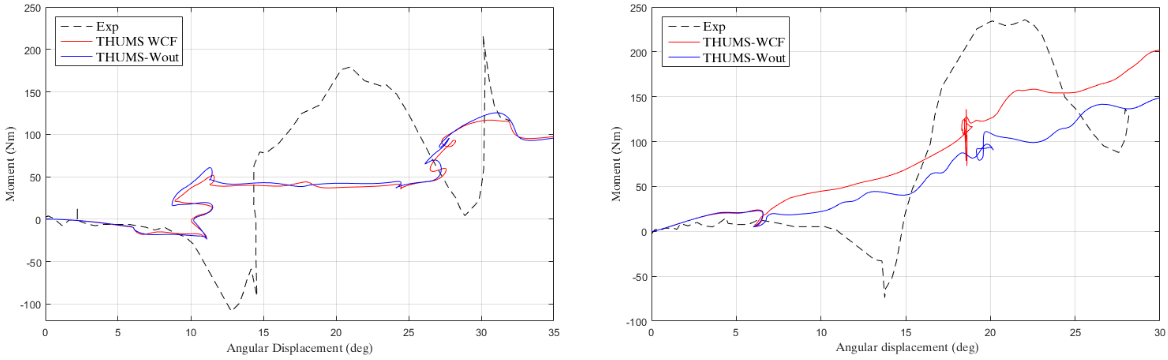

(a) Flexion **(b)** Extension

Figure 6.13: Moment vs angle response of T12-L5 model in THUMS with(red) and without(blue) intervertebral contact under dynamic flexion(a) and extension(b) tests

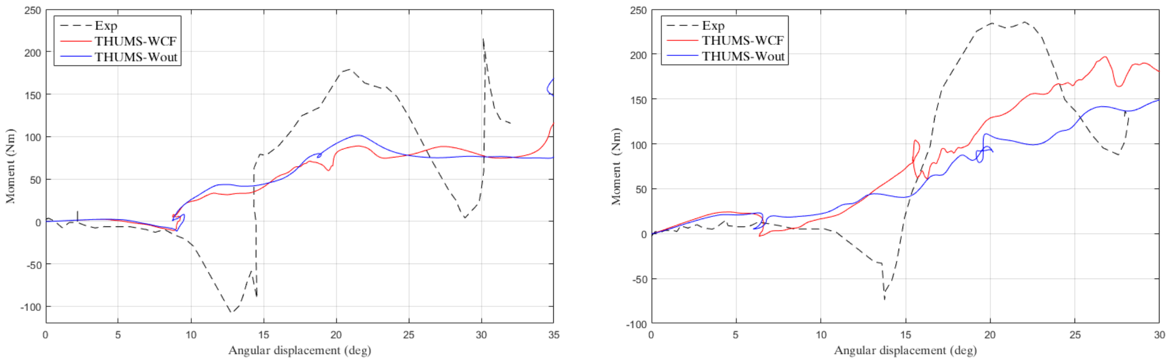

(a) Flexion **(b)** Extension

Figure 6.14: Moment vs angle response of T12-L5 model in THUMS with disc-1 with(red) and without(blue) intervertebral contact under dynamic flexion(a) and extension(b) tests

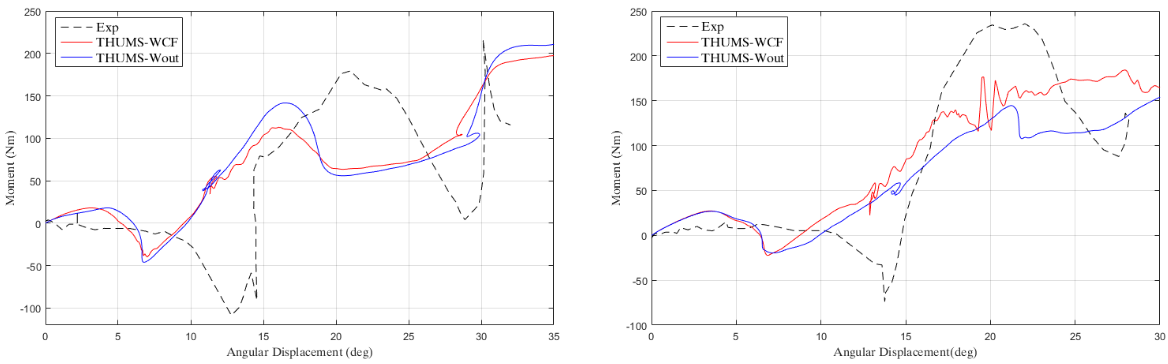

(a) Flexion **(b)** Extension

Figure 6.15: Moment vs angle response of T12-L5 model in THUMS with disc-2 with(red) and without(blue) intervertebral contact under dynamic flexion(a) and extension(b) tests

6.2.1 Flexion

THUMS response in flexion was different from the experimental results, Figure 6.13a. Nonetheless the model exhibited initial region of increased rotation with no moment, followed by negative moment and the final positive rise in moment as in the experiment [50]. Discrepancies begin early on when the peak negative moment in THUMS was limited to about 20 Nm at about 10°while for the experiment it reached a mean of -98.86 Nm before it curved upward at around 15°angular rotatation. Afterwards, THUMS exhibited a large increase in angular rotation without notable increase in moment and a large increase in moment with no notable increase in angular displacement. Peak value, measured at the same angular displacement was only 24% of the experimental result. At about 27°of angular rotation THUMS moment begin to rise while a fall in moment is observed for the cadaveric experiment as seen in Figure 6.13a. Dynamics of the model can be seen in Figures 6.16

When the discs were stiffned up, with disc-1, nature of the response curves changed compared to the original THUMS, as shown in Figure 6.14a. The peak value coincided with the experiment in time but was only 57.2% of the cadaveric experiment. There was no marked difference between the presence or absence of intervertebral contacts. Dynamics of the model can be seen in Figure 6.17.

With disc-2 the curve was improved but the angle offset was still present in the response, Figure 6.15a . Peak reaction moment occurred for smaller rotational angle in THUMS as compared to the cadaveric experiments and was slightly smaller (about 140 Nm) than the peak value for the cadaveric specimen (about 175 Nm). Otherwise it can be said that the dynamics of the cadaveric specimen were better mimicked in this model than all other disc models simulated in this experiment. Dynamics of the model are shown in Figure 6.18.

6.2.2 Extension

In this test THUMS failed to capture dynamic response of the cadavers. A slight improvement in dynamics of the model with disc-2 was observed, Figure 6.15b. Peak values occurred for the same angular rotations in THUMS and the experiment under extension loading. Reaction moment rose from 140 Nm in flexion to 170 Nm in extension as expected but the model response was still less stiff than the cadaveric specimen which peaked to about 230 Nm. This particular weakness in THUMS under extension test could be due to problems with the ligaments which are known to share large portion of the load under this mode [30] or could be due to the experimental set up.

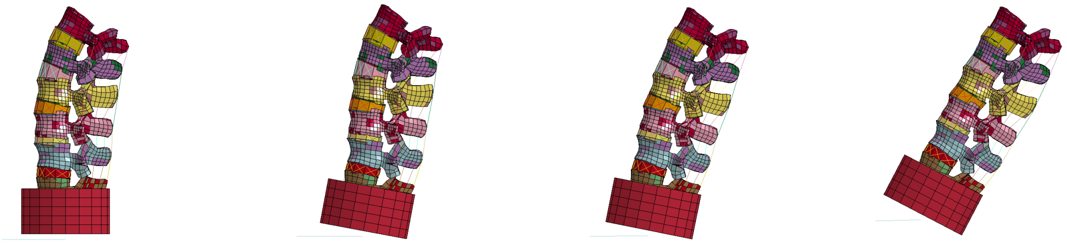

(a) 0 ms (b) 5 ms (c) 10 ms (d) 20 ms

Figure 6.16: Simulation of the T12-L5 model in THUMS with intervertebaral contact under dynamic flexion test [50]

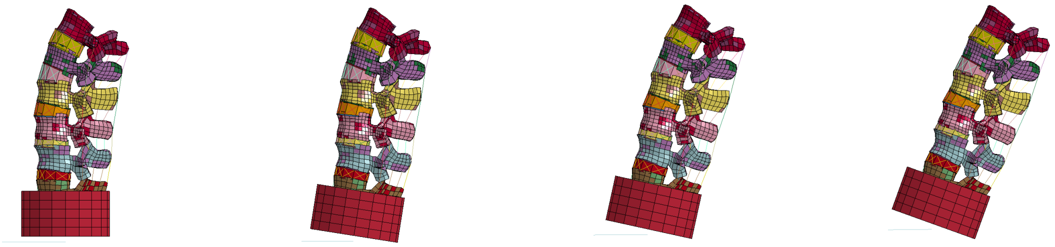

(a) 0 ms (b) 5 ms (c) 10 ms (d) 20 ms

Figure 6.17: Simulation of the T12-L5 model in THUMS with disc-1 and intervertebaral contact under dynamic flexion test [50]

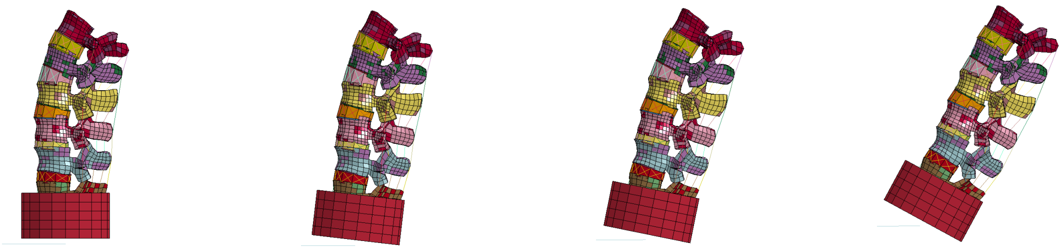

(a) 0 ms (b) 5 ms (c) 10 ms (d) 20 ms

Figure 6.18: Simulation of the T12-L5 model in THUMS with disc-2 and intervertebaral contact under dynamic flexion test [50]

6.3 Dynamic shear and flexion test

Samples responses are shown in Figure 6.19 where it is shown that the specimen exhibited linear increase in bending moment with time until peak acceleration was reached. Similarly, reaction moment was constant until it starts to decrease at failure point. THUMS, on the other hand, initially had a very low increase in bending moment distinctly different in shape from the experimental data, Figure 6.19. This initial nonlinear curve in THUMS was due to acceleration loading of the linear elastic disc material model. Contact forces manifested as a steep rise in the bending moment at about 52ms.

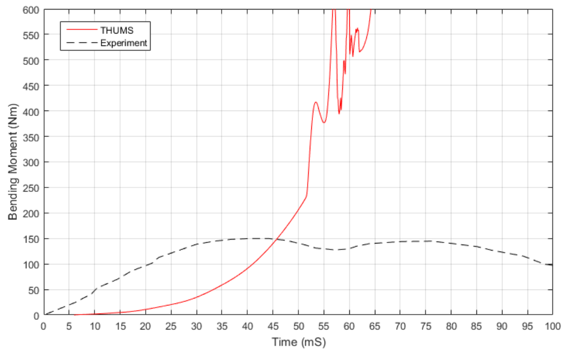

(a) Moderate Pulse

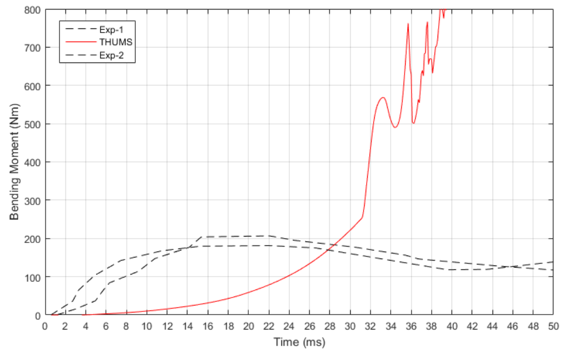

(b) Severe Pulse

Figure 6.19: Moment vs time sample response of lumbar FSUs in THUMS under coupled flexion and shear test

Under the moderate pulse, for the same flexion angle horizontal displacement in THUMS was within the experimental corridor, see table 6.1. Bending moment and shear force were about 2 and 4 times more in THUMS, respectively. Similarly vertical displacement was limited to about one seventh of the experimental result. First notable peak of contact force was visible at 52 ms. Failure flexion angles for THUMS occurred between 46 ms and 53 ms while for the experimental data it was between 40 ms and 60 ms. This data is tabulated in Table 6.1.

Table 6.1: Moment, shear, angle and displacement responses of the lumbar FSU in THUMS under the dynamic flexion and shear test [44]: Range of values stated for THUMS correspond to the lower and higher flexion angles in the experiments.

Response at Failure	Experiment data [44]		THUMS	
	Moderate	Severe	Moderate	Severe
Bending Moment(Nm)	120-160	150-215	150-425	400-550
Shear Force(KN)	0.385-0.53	0.525-0.715	1.3-2.50	3.75-6.75
Flexion Angle(deg)	11.3-16.1	16.3-21.2	11-16	16-21
Horizontal Displacment (mm)	4.9-8.3	6.9-10.1	5.5-8.5	8.5-9.5
Vertical Displacement (mm)	12.7-15.4	15.8-20.6	1.5-3.0	2.25-5.0

For test under the sever pulse two sample curves are shown in Figure 6.19b. For all the specimens failure occurred between 20 and 25ms at a flexion angle range between 16.3 and 21.2 degrees and a mean of 19.1 degrees. There was a large time offset between response of THUMS and the experiment hence flexion angle was used to compare the remaining parameters between THUMS and the experiments as in the moderate pulse test.

For the same flexion angle, under the severe pulse, shear force in THUMS was 8 times more and vertical displacement was limited to one sixths of that reported for the cadaveric specimens. Likewise bending moment was higher by a factor of 2.5. Only the horizontal displacement fell with in the experimental corridor see table 6.1. THUMS exhibited flexible response before contact forces were activated at 31 ms. The maximum and minimum flexion angles corresponded to 32 and 35 ms in THUMS. Hence the exaggerated results seen in THUMS are entirely due to the intervertebral contacts.

6.4 Static flexion and shear and flexion only tests

The results of this static experiment for specimens T12-L2 are tabulated in Table 6.2. Early in the coupled flexion and shear loading simulation THUMS exhibited lower stiffness. Later at about 13°of angular displacement contact forces between the upper two vertebral bodies caused a step rise in the load vs angle curve enabling all the response to fall inside the failure corridor, see Figure 6.20.

Table 6.2: Shear, flexion and compression responses of THUMS under static flexion and shear and flexion only tests [55]: Range of values stated for THUMS correspond to the lower and higher rotational displacement in the experiments.

		Experiment			THUMS		
Flexion and Anterior Shear							
Linear displ (mm)	Rot displ (deg)	Ant Shear(KN)	Flexion(NM)	Compr (KN)	Ant Shear (KN)	Flexion (Nm)	Compr (KN)
15.61±5.03	14.10±2.3	1.99±0.64	174.27±58.2	1.98±0.27	0.25-1.8	110-220	1.3-2.8
Flexion							
0.0	12.7±2.29	0.0	140.43±18.4	2.15±0.17	0.0	58-95	2.35-4

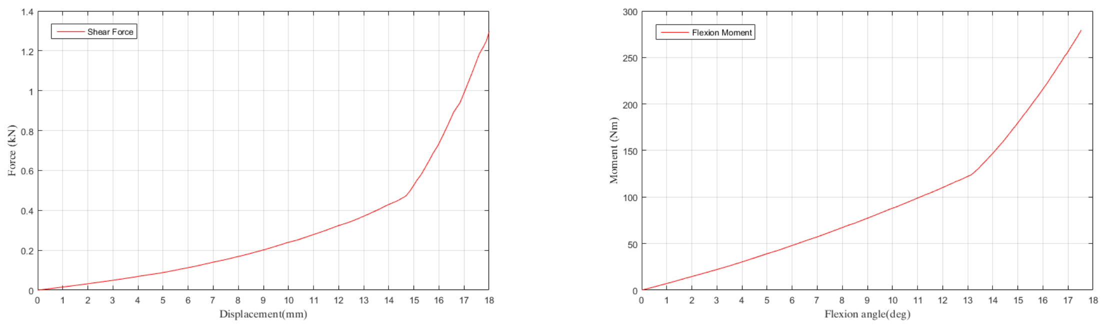

(a) Shear Force

(b) Flexion Moment

Figure 6.20: Shear/flexion vs displacement/angle response of THUMS under flexion and shear test [55] showing sudden change in slope due to intervertebral contacts

Flexion angle was used to compare the response of THUMS and the experimental data therefore in THUMS failure is considered as response at the same flexion angle as the experimental failure. For the flexion only loading, the reported failure flexion angle range was reached between 3 sec to 4 sec of simulation. Intervertebral Contact did not occur until 4.5 sec in time. Compressive force at the experimental failure point was found to be about 20% larger. On the contrary, the reaction moment in THUMS was about 50% less than that seen in the experiment. Hence response of the lumbar spine in THUMS under static flexion test is poor.

The use of discrete beam element to measure spinal forces was also demonstrated in this simulation. The result showed that the technique works correctly. This was verified against built in measurement tools in LS-PrePost. See Appendix A.4: Static flexion and shear and flexion only tests.

6.5 Ligaments test

Average length and average stiffness for each ligament type between T12 and S1 in experiment and in THUMS is tabulated in Table 6.3

Table 6.3: Cadaveric and THUMS ligament's average lengths and stiffness [67]

Ligaments	Length (mm)			Stiffness (Nmm^{-1})	
	Exp [67]		THUMS	Exp [67]	THUMS
	n	mean(STD)	mean(STD)	mean(STD)	mean(STD)
ALL	25	37.1(5.0)	32.39(5.0)	33.0(15.7)	21.44(12.26)
PLL	21	33.3(2.3)	32.42(4.75)	20.4(11.9)	12.15(3.82)
SSL	22	25.2(5.6)	33.60(5.70)	23.7(10.9)	23.55(7.4)
ISL	18	16.0(3.2)	16.63(5.55)	11.5(6.6)	10.93(3.45)
LF	22	15.2(1.3)	15.55(6.28)	27.2(9.2)	70.24(20.07)
CL	24	16.4(2.9)	5.50(1.55)	33.9(10.7)	29.23(9.19)

Majority of the ligament in THUMS are found to have similar average length and stiffness as the cadaveric counterparts, except for the CL and LF ligaments, see table 6.3. The CL ligament in THUMS was found to be about one third of human CL ligament in length. Similarly the LF ligament in THUMS was 2.58 times stiffer than its corresponding cadaveric ligament. Orientation of the ligaments might also to be different from the cadaveric ligaments, however, this information was not reported in the experiment.

6.6 GHBMC model

6.6.1 Dynamic compression test

6.6.1.1 FSU

The GHBMC lumbar model is found to be too flexible as compared to its cadaveric counterpart, see Figure 6.21. It is even too flexible as compared to THUMS. The response of the GHBMC is scaled up 5 times for visibility.

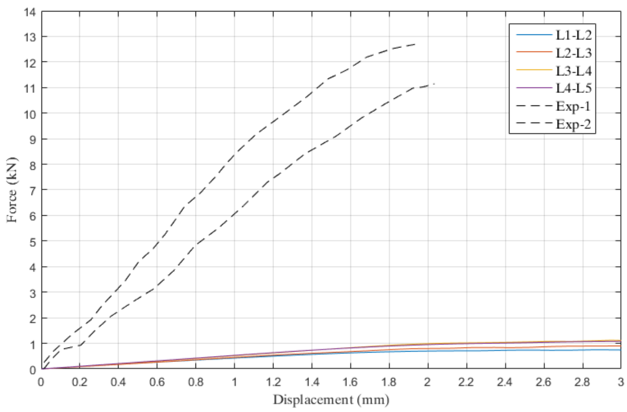

Figure 6.21: Force vs displacement response of GHBMC's lumbar FSUs (scaled 5 times) (L1-L2 = blue, L2-L3 = green, L3-L4 = red, L4-L5 = magenta) and the experimental corridor (dashed lines) under dynamic compression test [54]

6.6.1.2 T12-L5 segment

The response of the GHBMC lumbar model is too flexible, see Figure 6.22a and 6.22b. The response of the GHBMC is scaled up 5 times for visibility. The dynamics of the model during simulation is shown in Figure 6.23.

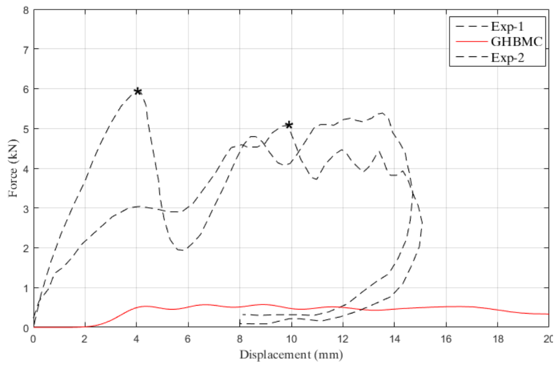

(a) Force vs vertical displacement

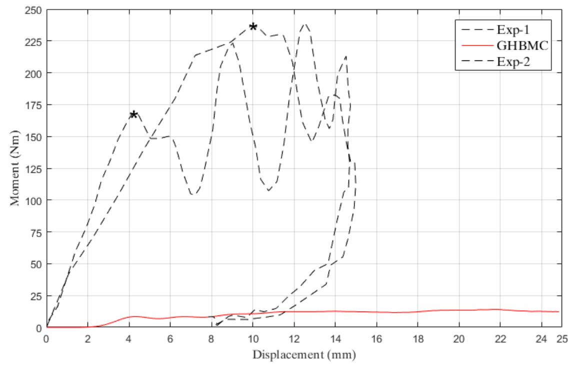

(b) Moment vs vertical displacement

Figure 6.22: Force vs displacement response of GHBMC lumbar spine (red) (scaled 5 times) and experimental corridor (dashed lines) under dynamic compression test [54]

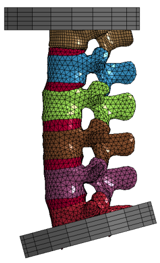

(a) 0 ms

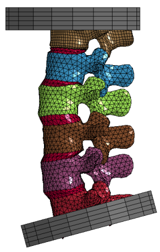

(b) 5 ms

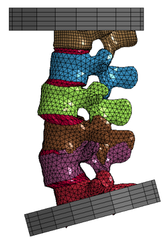

(c) 10 ms

Figure 6.23: Simulation of the T12-L5 model in GHBMC under dynamic compression test [54]

6.6.2 Dynamic flexion and extension tests

The GHMBC lumbar spine model failed to capture dynamics of the cadaveric counterpart as shown in Figures 6.24a and 6.24b. Moreover it is found to be too flexible. The plots shown in the Figure for GHBMC are scaled 10 times for visiblitiy. The dynamics of the model can be seen in Figure 6.25

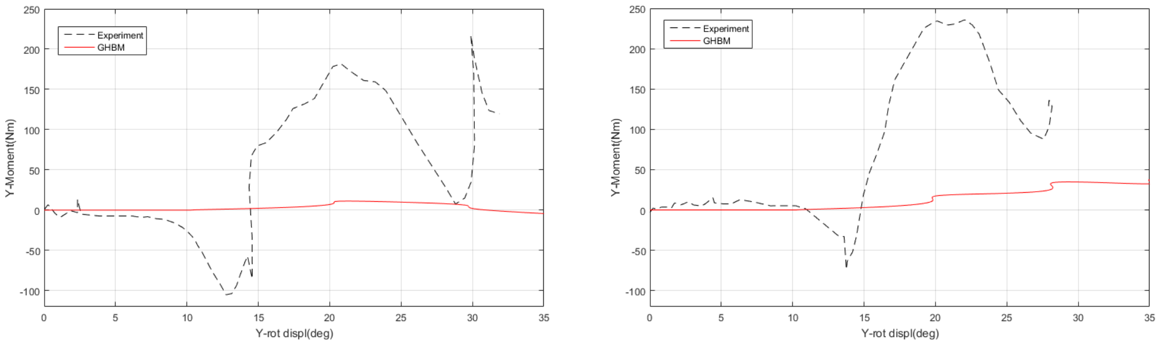

(a) Flexion vs Rotational displacement **(b)** Extension vs Rotational displacement

Figure 6.24: Moment vs angle response of GHBMC lumbar spine (red) (scaled 10 times) and experimental corridor (dashed line) under dynamic flexion and extension tests [50]

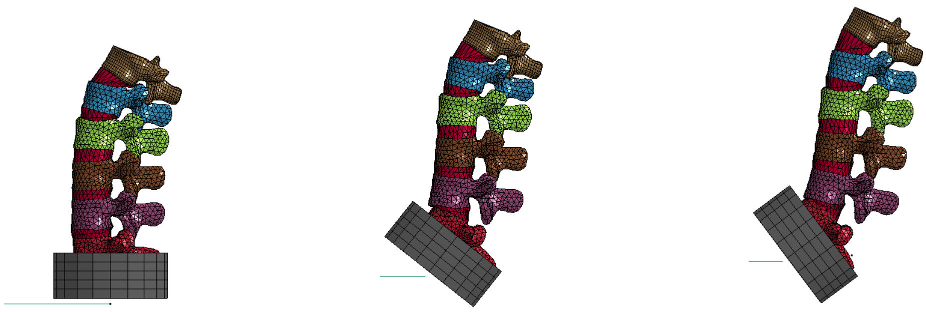

(a) 0 ms **(b)** 10 ms **(c)** 15 ms

Figure 6.25: Simulation of the T12-L5 model in GHBMC under dynamic flexion test [54]

7 Discussion

Of about 20 experiments collected in literature review, three dynamic and one static T12 to L5 experiments and one ligament test were simulated. Major loading modes were compression, tension flexion, extension and flexion coupled with shear loading. These are the prominent loading modes seen in MVC. Well defined thoracic or full cadaveric experiments were not found. Three intact cadaveric experiments were reviewed [30][58][59]. The first experiment [30] lacked clearly defined acceleration pulse and the reported data in the second and third experiments [58][59] were not relevant.

Response of the lumbar FSUs and T12-L5 model in THUMS under compression test [54] was found to be 3 to 4 times less stiffer than the cadaveric specimens. No force was carried by the ligaments or disc fibers except the CL ligament. The resulting lower stiffness is therefore due to the over flexible discs. The response of FSUs was improved by increasing Young's modulus of the discs, that is using disc-1.

The dynamic flexion and extension tests [50] is not failure experiment, hence dynamics of THUMS was correlated against experimental data as opposed to comparing the response only at failure point as in the remaining experiments. Large deviation of THUMS dynamics from cadaveric specimens were found under expreriment [50]. Peak moments were lower and occurred for smaller rotational displacements in THUMS. Nonetheless THUMS roughly recreated the two phases exhibited by the cadaveric specimens during the experiments.

In experiment [50], it was the linear displacement that was controlled but angular displacement was cross plotted against reaction moments. Thus the reported curves were more similar to the physiological motion [50]. This was responsible for the of highly nonlinear curves seen in THUMS' reponse as shown in figures in Section 6.2. As a result stiffness and peak moment were not calculated for THUMS. Because of the approach adapted in the experiment it is inconvenient to use this tests to evaluate THUMS.

Comparison against the ligament test [67] revealed too short CL and too stiff LF models in THUMS. The too short CL in THUMS suggest that the intervetebral gap at the articular processes could also be too small.

Only horizontal displacement was in good agreement with the experimental data during the dynamic flexion and shear test [44] . Higher reaction moments and shear forces were due to the intervertebral contacts. On the other hand the limited vertical displacement in THUMS was due to the short CL. The CL and LF ligaments in THUMS are tension only seatbelt elements orientated posteriorly from the lower to the upper vertebra at about 42°with respect to the horizontal. In this case, mainly tension is resisted and the specimen had it easier to translate anteriorly rather than vertically hence the limited vertical displacement. Similarly, the larger shear force could also be the due to the short CL. Substantial amount of force was carried by the CL ligaments in THUMS under the dyanamic flexion and shear loading.

THUMS achieved good correlation in compression force, anterior shear and flexion moments with the experimental data under the static flexion and shear loading [55]. Response of THUMS exhibited lower stiffness before intervertebral contact were activated and higher after the intervertebral contact were activated. The intertebral contact were entirely responsible for the achieved good correlation. Meanwhile THUMS response was poor in the flexion only static test. The discs in THUMS were observed to deform laterally without communicating moment. As the discs deform and the lower vertebra incline vertically, large shear force and lower flexion moment was recorded at the upper vertebra.

THUMS exhibited certain modeling weaknesses among which was the too small intevertebral gap. THUMS discs height is correct, however, greater length of the inververtebral discs in THUMS overlapp with the adjacent vertebral bodies leaving small inital gap. This gap is significantly smaller than what is reported in literature. This led to the unwanted response from the intervertebral contacts. This interference is pronounced under deflection exceeding about 5 mm and 12°of flexion or extensions in FSUs. This can be seen in Figure 6.3a and Tables 6.1 and 6.2 among others.

Good response was obtained for FSUs in THUMS under dynamic compression [54] with disc-1 and without intervetebral contacts. The same disc model failed to yield good response for the T12-L5 segment because of the buckling associated with longer segments. Intevertebral contact were insignificant with disc-2 in THUMS and the response was improved for the dynamic flexion and extension test [50] but not the dynamic compression test [54].

Validation of the THUMS cervical spine with muscles [23] revealed that improper muscle material model was responsible for the not bouncing back of the neck after frontal impact. The response was improved when the muscles were remodelled. It is reported that certain dynamics were still deviating from experimental data. The cervical spine in THUMS was validated good under some cases but lacked in other cases. The procedures adapted and the findings of this thesis report are similar to this ([23]) validation work.

The GHBMC's lumbar spine have been validated in flexion against cadaveric experimental data in full body [3]. The isolated lumbar spine from the GHBMC was evaluated in this thesis against the first two experiments and was found to be way too flexible as compared to THUMS. This suggests that the proper stiffness of the lumbar spine in this model could be due to the effect of neighbouring body parts and muscles. Similarly, THUMS response is expected to improve in full body tests.

On the other hand, the Spine Model for Safety and Surgery [6] (SM2S)'s lumbar model was validated against the same first two experiments [40] . The response is reported to be within the experimental corridor. The geometry and material property adapted in this model is detailed and different than THUMS but it hints that THUMS might require detailed remodelling. Moreover, the lumbar spine of the Takata human body model [74] was validated against the same two experiment and were found to be with in experimental corridor. The material properties in this model are similar to THUMS but had much higher Young's modulus for the elastic discs.

Finally, the material modeling of the discs, geometrical modeling of the intevertebral separation, ligaments' length and stiffness and contact forces are some of the major weaknesses identified in thoracolumbar spine in THUMS. Modifications should start by adapting further disc models for incorporating in to this THUMS model. Subsequent improvements might cover geometrical modifications of the intervertebral gap at the vertebral bodies as well as the articulating processes. Finer mesh of the discs and vertebral bones is also suggested to avoid vibrations and dips due to contact forces.

8 Conclusion

This evaluation work gave good insight in to the biofidelity of the thoracolumbar spine model in THUMS. Major weaknesses of the model were identified, possible causes stated and future improvements were directed.

THUMS' lumbar FSUs performed well in compression test with disc-1 and without interveterbral contacts but was lacking in all the remaining simulated tests. It was found that the stiffness of THUMS was not constant but varied depending on the intervertebral contacts. Therefore biofidelity of the thoracolumbar spine model in THUMS is concluded to be poor.

For a more biofidelic response, the disc material models, ligaments' stiffness and length and the intervertebral separation should be modified. The main weakness of the model is the intervertebral contact. Hence future modifications should pay enough attention to this critical modelling deficiency.

Bibliography

1. Iwamoto, M., Kisanuki, Y., Watanabe, I., *et al. Development of a finite element model of the total human model for safety (THUMS) and application to injury reconstruction* in *Proceedings of the International Research Council on the Biomechanics of Injury conference* **30** (2002), 12–p.
2. Shigeta, K., Kitagawa, Y. & Yasuki, T. *Development of next generation human FE model capable of organ injury prediction* in *Enhanced Safety of Vehicle Conference, Stuttgart, Germany, June* (2009), 15–18.
3. GHMBC, L. & Elemance, L. *GHBMC user manual: M50 occupant version 4.4 for LS-DYNA* (2015).
4. OF_TRANSPORTATION, U. *National Automotive Sampling System* http://www.nhtsa.gov/. 2016.
5. For the Advancement of Automotive Medicine, A. *about AIS* <`http://www.aaam.org/about-ais.html`> (2015).
6. Wagnac, E., Arnoux, P.-J., Garo, A., *et al. Calibration of hyperelastic material properties of the human lumbar intervertebral disc under fast dynamic compressive loads* **10,** 101007 (American Society of Mechanical Engineers, 2011).
7. Brolin, K. *Cervical Spine Injuries-Numerical Analyses and Statistical Survey* (Kungliga tekniska Högskolan, Institutionen för flygteknik, Doctoral thesis, 2002-29).
8. Peden, M., Scurfield, R., Sleet, D., *et al. World report on road traffic injury prevention* (World Health Organization Geneva, 2004).
9. Kopits, E. & Cropper, M. *Traffic fatalities and economic growth* **1,** 169–178 (Elsevier, 2005).
10. Yoganandan, N., Nahum, A. M., Melvin, J. W., *et al. Accidental Injury: Biomechanics and Prevention* (Springer, 2014).
11. Bohlin, N. *Safety belt device for vehicles* US Patent 3,147,995. Sept. 1964. <`https://www.google.com/patents/US3147995`>.
12. Jakobson, L., Bergman, T. & Johansson, L. *Identifying Thoracic and Lumbar Spinal Injuries in Car Accidents* in *Proceedings of the International Research Council on the Biomechanics of Injury conference* **34** (2006).
13. Pintar, F. A., Yoganandan, N., Maiman, D. J., *et al. Thoracolumbar spine fractures in frontal impact crashes* (2012).
14. Doud, A. N., Weaver, A. A., Talton, J. W., *et al. Has the incidence of thoracolumbar spine injuries increased in the United States from 1998 to 2011?* **1.** Springer, 297–304 (2015).

15. Richards, D., Carhart, M., Raasch, C., *et al. Incidence of thoracic and lumbar spine injuries for restrained occupants in frontal collisions* in *Annu Proc Assoc Adv Automot Med* **50** (2006), 125–139.

16. Griffith, H., Gleave, J. & Taylor, R. *Changing patterns of fracture in the dorsal and lumbar spine* **5492,** 891 (BMJ Group, 1966).

17. Inamasu, J. & Guiot, B. H. *Thoracolumbar junction injuries after motor vehicle collision: are there differences in restrained and nonrestrained front seat occupants?* (American Association of Neurological Surgeons, 2007).

18. Kifune, M., Panjabi, M., Arand, M., *et al. Fracture pattern and instability of thoracolumbar injuries* **2,** 98–103 (Springer, 1995).

19. King, A. I. in *Accidental Injury* 454–490 (Springer, 2002).

20. Forman, J. L., Lopez-Valdes, F. J., Duprey, S., *et al. The tolerance of the human body to automobile collision impact–a systematic review of injury biomechanics research, 1990–2009* 7–17 (Elsevier, 2015).

21. Yoganandan, N., Arun, M. W., Stemper, B. D., *et al. Biomechanics of human thoracolumbar spinal column trauma from vertical impact loading* 155 (Association for the Advancement of Automotive Medicine, 2013).

22. Oshita, F., Omori, K., Nakahira, Y., *et al. Development of a finite element model of the human body* in *7th International LS-DYNA Users Conference* **14** (2002), 205–212.

23. Chawla, A., Mukherjee, S., Mohan, D., *et al. Validation of the cervical spine model in THUMS* in *Proceedings of the 19th International Technical Conference on the Enhanced Safety of Vehicles Washington DC USA* (2005).

24. Mroz, K., Boström, O., Pipkorn, B., Wismans, J. & Brolin, K. *Comparison of Hybrid III and human body models in evaluating thoracic response for various seat belt and airbag loading conditions* in *IRCOBI Conference* (2010).

25. Pipkorn, B. & Kent, R. W. *Validation of a human body thorax model and its use for force, energy and strain analysis in various loading conditions* in *Proceedings of the International Research Council on the Biomechanics of Injury conference* **39** (2011), 210–223.

26. Kurutz, M. & Oroszváry, L. *Finite Element Modeling and Simulation of Healthy and Degenerated Human Lumbar Spine* (INTECH Open Access Publisher, 2012).

27. OpenStax. *Anatomy Physiology* <`https://creativecommons.org/licenses/by/3.0/`> (2013).

28. Bogduk, N. *Clinical anatomy of the lumbar spine and sacrum* (Elsevier Health Sciences, 2005).

29. Willen, J., Lindahl, S., Irstam, L., *et al. The Thoracolumbar Crush Fracture An Experimental Study on Instant Axial Dynamic Loading: The Resulting Fracture Type and Its Stability.* **6,** 624–631 (LWW, 1984).

30. Prasad, P., King, A. & Ewing, C. *The role of articular facets during+ Gz acceleration* **2,** 321–326 (American Society of Mechanical Engineers, 1974).

31. Begeman, P., King, A. I. & Prasad, P. *Spinal loads resulting from-Gdx acceleration* in *Proceedings: Stapp Car Crash Conference* **17** (1973).

32. Munjin, M. A., Zamorano, J. J., Marré, B., *et al. Speed hump spine fractures: injury mechanism and case series* **6,** 386–389 (LWW, 2011).

33. Bambach, M. R., Grzebieta, R. H. & McIntosh, A. *Thoracic injuries to contained and restrained occupants in single-vehicle pure rollover crashes* 115–121 (Elsevier, 2013).

34. Cannella, M., Pierce, C., Martin, K., *et al. Analysis of the mechanical behavior of the lumbar spine under high impact loading* in *Bioengineering Conference, Proceedings of the 2010 IEEE 36th Annual Northeast* (2010), 1–2.

35. Nicoll, E. *Fractures of the dorso-lumbar spine* **3,** 376–394 (British Editorial Society of Bone and Joint Surgery, 1949).

36. Bricknell, M. & Craig, S. C. *Military parachuting injuries: a literature review* **1,** 17–26 (Soc Occupational Med, 1999).

37. Langrana, N., Harten Jr, R., Lin, D., *et al. Acute thoracolumbar burst fractures: a new view of loading mechanisms* **5,** 498–508 (LWW, 2002).

38. Xu, L., Jensen, J., Byrnes, K., *et al. Comparative performance evaluation of THOR and hybrid III* tech. rep. (SAE Technical Paper, 2000).

39. Ball, S. T., Vaccaro, A. R., Albert, T. J., *et al. Injuries of the thoracolumbar spine associated with restraint use in head-on motor vehicle accidents* **4,** 297–304 (LWW, 2000).

40. Wang, M. C., Pintar, F., Yoganandan, N., *et al. The continued burden of spine fractures after motor vehicle crashes: clinical article* **2,** 86–92 (American Association of Neurological Surgeons, 2009).

41. Rao, R. D., Berry, C. A., Yoganandan, N., *et al. Occupant and crash characteristics in thoracic and lumbar spine injuries resulting from motor vehicle collisions* **10,** 2355–2365 (Elsevier, 2014).

42. Baudrit, P., Potier, P., Petit, P., *et al. Cadaver and dummy investigation of injury risk with anti-sliding system in case of static deployment* in *19th International Technical Conference on the Enhanced Safety of Vehicles* (2005).

43. Neumann, P., Keller, T., Ekström, L., *et al. Mechanical properties of the human lumbar anterior longitudinal ligament* **10,** 1185–1194 (Elsevier, 1992).

44. Osvalder, A.-L., Neumann, P., Lövsund, P., *et al. A method for studying the biomechanical load response of the (in vitro) lumbar spine under dynamic flexion-shear loads* **10,** 1227–1236 (Elsevier, 1993).

45. Neumann, P., Nordwall, A. & Osvalder, A. *Traumatic Instability of the Lumbar Spine: A Dynamic In Vitro Study of Flexion-Distraction Injury.* **10,** 1111–1120 (LWW, 1995).

46. Ochia, R. S., Tencer, A. F. & Ching, R. P. *Effect of loading rate on endplate and vertebral body strength in human lumbar vertebrae* **12,** 1875–1881 (Elsevier, 2003).

47. Demetropoulos, C. K., Yang, K. H., Grimm, M. J., *et al. Mechanical properties of the cadaveric and Hybrid III lumbar spines* tech. rep. (SAE Technical Paper, 983160, 1998).

48. Stemper, B. D., Storvik, S. G., Yoganandan, N., *et al. A new PMHS model for lumbar spine injuries during vertical acceleration* **8,** 081002 (American Society of Mechanical Engineers, 2011).

49. Panjabi, M. M., Kifune, M., Arand, M., *et al.* Validity of the Three-Column Theory of Thoracolumbar Fractures: A Biomechanic Investigation. *Spine* **20,** 1122–1127 (1995).

50. Demetropoulos, C. K., Yang, K. H., Grimm, M. J., *et al. High rate mechanical properties of the Hybrid III and cadaveric lumbar spines in flexion and extension* tech. rep. (SAE Technical Paper, 99SC18, 1999).

51. Schultz, A., Warwick, D., Berkson, M., *et al. Mechanical properties of human lumbar spine motion segments—Part I: Responses in flexion, extension, lateral bending, and torsion* **1,** 46–52 (American Society of Mechanical Engineers, 1979).

52. Denis, F. *The three column spine and its significance in the classification of acute thoracolumbar spinal injuries.* **8,** 817–831 (LWW, 1983).

53. Magerl, F., Aebi, M., Gertzbein, S., *et al. A comprehensive classification of thoracic and lumbar injuries* **4,** 184–201 (Springer, 1994).

54. Duma, S. M., Kemper, A. R., McNeely, D. M., *et al. Biomechanical response of the lumbar spine in dynamic compression.* 476–481 (2005).

55. Belwadi, A. & Yang, K. H. *Cadaveric lumbar spine responses to flexion with and without anterior shear displacement* in *Proceedings of the International Reseach Council on the Biomechanics of Injury conference* **36** (2008), 397–410.

56. Myklebust, J., Sances Jr, A., Maiman, D., *et al. Experimental spinal trauma studies in the human and monkey cadaver* tech. rep. (DTIC Document, 1982).

57. Sances, A. *Mechanisms of head and spine trauma* (Aloray Pub, 1986).

58. King, A. I. & Vulcan, A. P. *Elastic deformation characteristics of the spine* **5,** 413–429 (Elsevier, 1971).

59. Luet, C., Trosseille, X., Drazétic, P., *et al. Kinematics and Dynamics of the Pelvis in the Process of Submarining using PMHS Sled Tests* 411 (The Stapp Association, 2012).

60. Garges, K. J., Nourbakhsh, A., Morris, R., *et al. A comparison of the torsional stiffness of the lumbar spine in flexion and extension* **8,** 563–569 (Elsevier, 2008).

61. Begeman, P., Visarius, H., Nolte, L.-P., *et al. Visocelastic shear responses of the cadaver and Hybrid III lumbar spine* tech. rep. (SAE Technical Paper, 1994).

62. Stemper, B. D., Board, D., Yoganandan, N., *et al. Biomechanical properties of human thoracic spine disc segments* **1,** 18 (Medknow Publications, 2010).

63. Schendel, M. J., Wood, K. B., Buttermann, G. R., *et al. Experimental measurement of ligament force, facet force, and segment motion in the human lumbar spine* **4-5,** 427–438 (Elsevier, 1993).

64. Yoganandan, N., Cusick, J. F., Pintar, F. A., Droese, K., *et al. Cyclic compression-flexion loading of the human lumbar spine.* **7,** 784–790 (LWW, 1994).

65. Yoganandan, N., Mykiebust, J. B., Cusick, J. F., *et al. Functional biomechanics of the thoracolumbar vertebral cortex* **1,** 11–18 (Elsevier, 1988).

66. Yamamoto, I., Panjabi, M. M., Crisco, T., *et al. Three-dimensional movements of the whole lumbar spine and lumbosacral joint.* **11,** 1256–1260 (LWW, 1989).

67. Pintar, F. A., Yoganandan, N., Myers, T., *et al. Biomechanical properties of human lumbar spine ligaments* **11,** 1351–1356 (Elsevier, 1992).

68. Watanabe, I., Furusu, K., Kato, C., *et al. Development of practical and simplified human whole body FEM model* **2,** 189–194 (Elsevier, 2001).

69. Iwamoto, M., Nakahira, Y. & Kimpara, H. *Development and Validation of the Total HUman Model for Safety (THUMS) Toward Further Understanding of Occupant Injury Mechanisms in Precrash and During Crash* **sup1,** S36–S48 (Taylor & Francis, 2015).

70. Osvalder, A.-L., Neumann, P., Lövsund, P. & Nordwall, A. *Ultimate strength of the lumbar spine in flexion—an in vitro study* **5,** 453–460 (Elsevier, 1990).

71. Östh, J., Brolin, K., Svensson, M. Y., *et al. A Female Ligamentous Cervical Spine Finite Element Model Validated for Physiological Loads* **6,** 061005 (American Society of Mechanical Engineers, 2016).

72. Panzer, M. B. & Cronin, D. S. *C4–C5 segment finite element model development, validation, and load-sharing investigation* **4,** 480–490 (Elsevier, 2009).

73. Iatridis, J. C., Weidenbaum, M., Setton, L. A., *et al. Is the nucleus pulposus a solid or a fluid? Mechanical behaviors of the nucleus pulposus of the human intervertebral disc* **10,** 1174–1184 (LWW, 1996).

74. Zhang, N. & Zhao, J. *Study of Compression-Related Lumbar Spine Fracture Criteria Using a Full Body FE Human Model* in *23rd International Technical Conference on the Enhanced Safety of Vehicles (ESV)* (2013).

Appendices

A:Simulation Cards

A1. Dynamic compression test [54]

FSU

$*BOUNDARY_PRESCRIBED_MOTION_RIGID_ID
$ id heading
01m_s_Compression_L1
$ pid dof vad lcid sf vid death birth
41961842 3 0 44000100 -1.0 01.00000E28 0.0
$$ id 10 heading
Lower_potting_Z_constrained
$ pid dof vad lcid sf vid death birth
41961841 3 2 44000101 1.0 01.00000E28 0.0
$ id hspace10 heading
Lower_potting_X_constrained
$ pid dof vad lcid sf vid death birth
41961841 1 2 44000101 1.0 01.00000E28 0.0
$ id heading
Lower_potting_Y_constrained
$ pid dof vad lcid sf vid death birth
41961841 2 2 44000101 1.0 01.00000E28 0.0
$ id heading
Lower_potting_XRot_constrained
$ pid dof vad lcid sf vid death birth
41961841 5 2 44000101 1.0 01.00000E28 0.0
$ id heading
Lower_potting_YRot_constrained
$ pid dof vad lcid sf vid death birth
41961841 6 2 44000101 1.0 01.00000E28 0.0
$ id heading
Lower_potting_ZRot_constrained
$ pid dof vad lcid sf vid death birth
41961841 7 2 44000101 1.0 01.00000E28 0.0
$*BOUNDARY_SPC_SET_ID
$ id heading
L1_5DOF_Constrained
$ nsid cid dofx dofy dofz dofrx dofry dofrz
2 0 1 1 0 1 1 1
$*CONSTRAINED_RIGID_BODIES
pidm pids iflag

41330000 41330010 0
$41330000 41930275 0 $

T12-L5 segment

$*BOUNDARY_PRESCRIBED_MOTION_RIGID_ID
$ id heading
Upper_pot_compr_1m_s
$ pid dof vad lcid sf vid death birth
41962462 3 0 44000100 -1.000000 01.0000E+28 0.000
$$ id heading
Lower_pot_const_x
$ pid dof vad lcid sf vid death birth
41962461 1 2 44000101 1.000000 01.0000E+28 0.000
$ id heading
Lower_pot_const_y
$ pid dof vad lcid sf vid death birth
41962461 2 2 44000101 1.000000 01.0000E+28 0.000
$ id heading
Lower_pot_const_z
$ pid dof vad lcid sf vid death birth
41962461 3 2 44000101 1.000000 01.0000E+28 0.000
$ id heading
Lower_pot_const_rotx
$ pid dof vad lcid sf vid death birth
41962461 5 2 44000101 1.000000 01.0000E+28 0.000
$ id heading
Lower_pot_const_roty
$ pid dof vad lcid sf vid death birth
41962461 6 2 44000101 1.000000 01.0000E+28 0.000
$ id heading
Lower_pot_const_rotz
$ pid dof vad lcid sf vid death birth
41962461 7 2 44000101 1.000000 01.0000E+28 0.000
$ id heading
Upper_pot_const_x
$ pid dof vad lcid sf vid death birth
41962462 1 2 44000101 1.000000 01.0000E+28 0.000
$ id heading
Upper_pot_const_y
$ pid dof vad lcid sf vid death birth
41962462 2 2 44000101 1.000000 01.0000E+28 0.000
$ id heading
Upper_pot_const_rotx
$ pid dof vad lcid sf vid death birth
41962462 5 0 44000101 1.000000 01.0000E+28 0.000
$ id heading
Upper_pot_const_roty
$ pid dof vad lcid sf vid death birth
41962462 6 2 44000101 1.000000 01.0000E+28 0.000
$ id heading

Upper_pot_const_rotz
$ pid dof vad lcid sf vid death birth
41962462 7 2 44000101 1.000000 01.0000E+28 0.000

$$*CONSTRAINED_RIGID_BODIES
$ pidm pids iflag
41962461 41330400 0 $$41962462 41911100 0 $$
$$$

A2. Dynamic flexion and extension tests [50]

Flexion

$*BOUNDARY_PRESCRIBED_MOTION_RIGID_ID
$ id heading
L5_Constr_x
$ pid dof vad lcid sf vid death birth
41330400 1 2 44000101 1.0 01.00000E28 0.0
$ id heading
L5_constr_y
$ pid dof vad lcid sf vid death birth
41330400 2 2 44000101 1.0 01.00000E28 0.0
$ id heading
L5_constr_z
$ pid dof vad lcid sf vid death birth
41330400 3 2 44000101 1.0 01.00000E28 0.0
$ id heading
L5_constr_rotx
$ pid dof vad lcid sf vid death birth
41330400 5 2 44000101 1.0 01.00000E28 0.0
$ id heading
L5_constr_roty
$ pid dof vad lcid sf vid death birth
41330400 6 2 44000101 1.0 01.00000E28 0.0
$ id heading
L5_constr_rotz
$ pid dof vad lcid sf vid death birth
41330400 7 2 44000101 1.0 01.00000E28 0.0
$ id heading
$potting_constr_ydisp
$ pid dof vad lcid sf vid death birth
41961851 2 2 44000101 1.0 01.00000E28 0.0
$ id heading
potting_constr_xrot
$ pid dof vad lcid sf vid death birth
41961851 5 2 44000101 1.0 01.00000E28 0.0
$ id heading
potting_constr_zrot
$ pid dof vad lcid sf vid death birth
41961851 7 2 44000101 1.0 01.00000E28 0.0

$*BOUNDARY_PRESCRIBED_MOTION_NODE_ID
$ id heading
steel_cable_distal_node
$ nid dof vad lcid sf vid death birth
41931740 1 0 44000100 1.0 01.00000E28 0.0
$*BOUNDARY_SPC_NODE
$ nid cid dofx dofy dofz dofrx dofry dofrz
41931740 0 0 1 1 1 1 1
$*LOAD_BODY_Z
$ lcid sf lciddr xc yc zc cid
44000102 -1.0 0 0.0 0.0 0.0 0

$*DEFINE_CURVE_TITLE
load_4m_s
$ lcid sidr sfa sfo offa offo dattyp lcint
44000100 0 1.0 1.0 0.0 0.0 0 0
$ a1 o1
0.0 2.0
3.0 4.0
50.0 4.0
*DEFINE_CURVE_TITLE
zero_curve
$ lcid sidr sfa sfo offa offo dattyp lcint
44000101 0 1.0 1.0 0.0 0.0 0 0
$ a1 o1
0.0 0.0
50.0 0.0
*DEFINE_CURVE_TITLE
gravity
$ lcid sidr sfa sfo offa offo dattyp lcint
44000102 0 1.0 1.0 0.0 0.0 0 0
$ a1 o1
0.0 0.00986
50.0 0.00986

$*CONSTRAINED_EXTRA_NODES_NODE
$ pid nid iflag
41961851 41931739 0
*CONSTRAINED_RIGID_BODIES
$ pidm pids iflag
41961851 41911100 0

Extension

The same setting as above. Only the specimen was rotated 180degrees

A3. Dynamic flexion and shear test [44]

$*CONSTRAINED_RIGID_BODIES
$ pidm pids iflag
41961842 41330010 0
41961841 41330110 0
41961846 41961843 0
41961843 41961842 0
41961847 41961841 0

$*BOUNDARY_PRESCRIBED_MOTION_RIGID_ID
$ id heading
0Pendulum_acceleration
$ pid dof vad lcid sf vid death birth
41961846 1 1 44000102 1.0 01.00000E28 0.0

$$
*BOUNDARY_PRESCRIBED_MOTION_RIGID_ID
$ id heading
Const_LowerpotLoadCell_pot_x
$ pid dof vad lcid sf vid death birth
41961847 1 2 44000101 1.0 01.00000E28 0.0
$ id heading
Const_LowerpotLoadCell_pot_y
$ pid dof vad lcid sf vid death birth
41961847 2 2 44000101 1.0 01.00000E28 0.0
$ id heading
Const_LowerpotLoadCell_pot_z
$ pid dof vad lcid sf vid death birth
41961847 3 2 44000101 1.0 01.00000E28 0.0
$ id heading
Const_LowerpotLoadCell_pot_xrot
$ pid dof vad lcid sf vid death birth
41961847 5 2 44000101 1.0 01.00000E28 0.0
$ id heading
Const_LowerpotLoadCell_pot_yrot
$ pid dof vad lcid sf vid death birth
41961847 6 2 44000101 1.0 01.00000E28 0.0
$ id heading
Const_LowerpotLoadCell_pot_zrot
$ pid dof vad lcid sf vid death birth
41961847 7 2 44000101 1.0 01.00000E28 0.0
$
*BOUNDARY_PRESCRIBED_MOTION_RIGID_ID
$ id heading
Const_upper_pot_ydispl
$ pid dof vad lcid sf vid death birth
41961842 2 2 44000101 1.0 01.00000E28 0.0
$ id heading
Const_upper_pot_rotx
$ pid dof vad lcid sf vid death birth

41961842 5 2 44000101 1.0 01.00000E28 0.0
$ id heading
Const_upper_pot_rotz
$ pid dof vad lcid sf vid death birth
41961842 7 2 44000101 1.0 01.00000E28 0.0
$*LOAD_BODY_Z
$ lcid sf lciddr xc yc zc cid
44000103 -1.0 0-86.036598 2.3347499 209.127 0

$*DEFINE_CURVE_TITLE
zero_load $$ lcid sidr sfa sfo offa offo dattyp lcint
44000101 0 1.0 1.0 0.0 0.0 0 0
$ a1 o1
0.0 0.0
250.0 0.0
*DEFINE_CURVE_TITLE
Severe_pulse
$ lcid sidr sfa sfo offa offo dattyp lcint
44000102 0 1.0 0.00981 0.0 0.0 0 0
$ a1 o1
0.0 0.0
20.0 0.0
21.875 1.20000005
36.875 10.80000019
38.75 12.0
270.0 12.0
*DEFINE_CURVE_TITLE
moderate_pulse
$ lcid sidr sfa sfo offa offo dattyp lcint
44000102 0 1.0 0.00981 0.0 0.0 0 0
$ a1 o1
0.0 0.0
20.0 0.0
23.75 0.5
53.75 4.5
57.5 5.0
170.0 5.0
*DEFINE_CURVE_TITLE
gravity
$ lcid sidr sfa sfo offa offo dattyp lcint
44000103 0 1.0 0.0098 0.0 0.0 0 0
$ a1 o1
0.0 1.0
250.0 1.0

A4. Static flexion and shear and flexion only tests [55]

$*BOUNDARY_PRESCRIBED_MOTION_RIGID_ID
$ id heading

2flexion
$ pid dof vad lcid sf vid death birth
41962461 6 0 44000100 1.0 0 0.0 0.0

$*BOUNDARY_PRESCRIBED_MOTION_RIGID_LOCAL_ID
$ id heading
1ant_shear
$ pid dof vad lcid sf vid death birth
41962461 1 0 44000101 -1.0 0 0.0 0.0

*BOUNDARY_PRESCRIBED_MOTION_RIGID_ID
$ id heading
2flexion
$ pid dof vad lcid sf vid death birth
41962461 6 0 44000100 1.0 0 0.0 0.0

$
*MAT_RIGID_TITLE
Alu_potting upper
$ mid ro e pr n couple m alias
419618492.70000E-6 68.9000020.33000001 0.0 0.0 0.0
$ cmo con1 con2
1.0 7 7
$lco or a1 a2 a3 v1 v2 v3
0.0 0.0 0.0 0.0 0.0 0.0

*MAT_RIGID_TITLE
Aluminum_potting lower
$ mid ro e pr n couple m alias
419618522.70000E-6 68.9000020.33000001 0.0 0.0 0.0
$ cmo con1 con2
1.0 4 6
$lco or a1 a2 a3 v1 v2 v3
0.0 0.0 0.0 0.0 0.0 0.0

$ vol iner cid ca offset rrcon srcon trcon
1.0 1.0 1 0.0 0.0 0.0 0.0 0.0
*MAT_LINEAR_ELASTIC_DISCRETE_BEAM_TITLE
load_cell
$ mid ro tkr tks tkt rkr rks rkt
41961851 0.01 1000.0 1000.0 1000.0 1000000.0 1000000.0 1000000.0
$ tdr tds tdt rdr rds rdt
0.0 0.0 0.0 0.0 0.0 0.0
$ for fos fot mor mos mot
0.0 0.0 0.0 0.0 0.0 0.0
*SECTION_BEAM_TITLE
LOAD_CELL
$ secid elform shrf qr/irid cst scoor nsm
41962464 6 0.0 0 0 0.0 0.0

$*DEFINE_COORDINATE_NODES_TITLE

LOAD_CELL_coord_AT_upper_potting
$ cid n1 n2 n3 flag dir
1 50 30 40 1X
*DEFINE_COORDINATE_NODES_TITLE
COORD_at_lower_potting_for_shear
$ cid n1 n2 n3 flag dir
2 100 200 300 1X

*DEFINE_CURVE_TITLE $3.5deg/sec
$ lcid sidr sfa sfo offa offo dattyp lcint
44000100 0 1.0 1.0 0.0 0.0 0 0
$ a1 o1
0.0 6.100000e-005
10000.0 6.100000e-005
*DEFINE_CURVE_TITLE $4mm/s
$ lcid sidr sfa sfo offa offo dattyp lcint
44000101 0 1.0 1.0 0.0 0.0 0 0
$ a1 o1
0.0 0.004
10000.0 0.004
*DEFINE_CURVE_TITLE
zero curve
$ lcid sidr sfa sfo offa offo dattyp lcint
44000102 0 1.0 1.0 0.0 0.0 0 0
$ a1 o1
0.0 0.0
10000.0 0.0

$*SET_NODE_LIST_TITLE
loadcell_coord_sys_nodes
$ sid da1 da2 da3 da4 solver
1 0.0 0.0 0.0 0.0MECH
$ nid1 nid2 nid3 nid4 nid5 nid6 nid7 nid8
30 40 0 0 0 0 0 0
*SET_NODE_LIST_TITLE
shear_coord_nodes
$ sid da1 da2 da3 da4 solver
2 0.0 0.0 0.0 0.0MECH
$ nid1 nid2 nid3 nid4 nid5 nid6 nid7 nid8
100 200 300 0 0 0 0 0

$*CONSTRAINED_EXTRA_NODES_NODE
$$ANSA_ID;2;
$ pid nid iflag
41330100 10 0
$ANSA_ID;3;
41962462 20 0

*CONSTRAINED_EXTRA_NODES_SET
$$ANSA_ID;1;
$ pid nsid iflag

41330100 1 0
*CONSTRAINED_EXTRA_NODES_SET
$ANSA_ID;4;
$ pid nsid iflag
41962461 2 0
*CONSTRAINED_RIGID_BODIES
$$ANSA_ID;5;
$ pidm pids iflag
41962461 41911100 0

$*BOUNDARY_PRESCRIBED_MOTION_RIGID_ID
$ id heading
Lower_pot_fix_y_translation
$ pid dof vad lcid sf vid death birth
41962461 2 0 44000102 1.0 01.00000E28 0.0

A5. Material and section cards for THUMS, disc-1 and disc-2

original THUMS

See Appendix A tables **??** and **??**

Elastic disc material with increased Young's modulus (Disc-1)

*MAT_ELASTIC_TITLE
$Mat_Nucleus
$ mid ro e pr da db not used
419301501.00000E-6 0.0010.49900001 0.0 0.0 0
*SECTION_SOLID
$ secid elform aet
41930190 2 0

*MAT_ELASTIC_TITLE
$Mat_Annulus_in
$ mid ro e pr da db not used
419301601.00000E-6 0.0040.40000001 0.0 0.0 0
*SECTION_SOLID
$ secid elform aet
41930160 2 0

*MAT_ELASTIC_TITLE
$Mat_Annulus_out
$ mid ro e pr da db not used
419301901.00000E-6 0.0040.40000001 0.0 0.0 0
*SECTION_SOLID
$ secid elform aet
41930190 2 0

Viscoelastic and Hill-Foam material (Disc-2)

*MAT_VISCOELASTIC_TITLE
Viscous_Nucleus
$ mid ro bulk g0 gi beta
419618421.00000E-6 1.721.78000E-57.10000E-6 1.0
*SECTION_SOLID
$ secid elform aet
41930200 2 0

*MAT_HILL_FOAM_TITLE
Hill_Annulus_in
$ mid ro k n nu lcid fittype lcsr
419618431.00000E-63.38300E-4 2.0 0.0 0 1 0
$ c1 c2 c3 c4 c5 c6 c7 c8
1.15000E-4 0.002101-8.9300E-4 0.0 0.0 0.0 0.0 0.0
$ b1 b2 b3 b4 b5 b6 b7 b8
4.0 -1.0 -2.0 0.0 0.0 0.0 0.0 0.0
$ r m
0.0 0.0
*SECTION_SOLID
$ secid elform aet
41930210 2 0

*MAT_HILL_FOAM_TITLE
Hill_Annulus_out
$ mid ro k n nu lcid fittype lcsr
419618441.00000E-63.38300E-4 2.0 0.0 0 1 0
$ c1 c2 c3 c4 c5 c6 c7 c8
1.15000E-4 0.002101-8.9300E-4 0.0 0.0 0.0 0.0 0.0
$ b1 b2 b3 b4 b5 b6 b7 b8
4.0 -1.0 -2.0 0.0 0.0 0.0 0.0 0.0
$ r m
0.0 0.0
*SECTION_SOLID
$ secid elform aet
41930210 2 0